© 2015. Published by The Company of Biologists Ltd | Development (2015) 142, 544-554 doi:10.1242/dev.115444

RESEARCH ARTICLE

Surrounding tissues canalize motile cardiopharyngeal progenitors towards collective polarity and directed migration

Stephanie Gline, Nicole Kaplan, Yelena Bernadskaya, Yusuff Abdu* and Lionel Christiaen‡

ABSTRACT

Collectively migrating cells maintain group polarity and interpret external cues to reach their destination. The cardiogenic progenitors (also known as trunk ventral cells, TVCs) of the ascidian *Ciona intestinalis* provide a simple chordate model with which to study collective migration. Bilateral pairs of associated TVCs undergo a stereotyped polarized migration away from the tail towards the ventral trunk, arguably constituting the simplest possible example of directed collective migration. To identify tissues contributing to TVC polarity and migration, we quantified the contact between TVCs and surrounding tissues, and blocked the secretory pathway in a tissue-specific manner. Even though TVCs normally migrate as an invariably determined leader-trailer polarized pair of adherent cells, they are capable of migrating individually, albeit a shorter distance and with altered morphology. The mesenchyme contacts newborn TVCs and contributes to robust specification of the trailer but appears to have only minor effects on directed migration. The notochord does not contact the TVCs but contributes to the onset of migration. The trunk endoderm first contacts the leader TVC, then 'encases' both migrating cells and provides the inputs maintaining leader-trailer polarity. Migrating TVCs adhere to the epidermis and need this contact for their cohesion. These phenomenological studies reveal that inherently motile cardiopharyngeal progenitors are channeled into stereotyped behaviors by interactions with surrounding tissues.

KEY WORDS: *Ciona*, Collective cell migration, Collective cell polarity, Cardiogenic progenitors, Live imaging, Trunk ventral cells

INTRODUCTION

Collective cell migration involves cell groups of variable size, shape and degree of connectivity that move towards a common destination (Rørth, 2012). Collective cell migrations play a fundamental role in a wide range of developmental and pathological processes, including gastrulation, neural crest migration, angiogenesis, wound healing and cancer metastasis (Aman and Piotrowski, 2010; Friedl and Gilmour, 2009). The collective population polarizes into leaders and followers, which often correspond to distinct cell states within homogeneous populations (Rørth, 2012). During directed migration, cells respond to combinations of attractive and repellent signals, as well as to physical and mechanical constraints imposed by their surrounding environment. The migrating population must integrate these molecular and mechanical cues to collectively polarize and reach their destination. How populations of cells achieve this has been a long-standing issue of cell and developmental biologists.

Collectively migrating cells can form: (1) tightly associated epithelia with generally stable cell positions, as in the zebrafish lateral line primordium (LLP); (2) loosely and dynamically migrating streams of mesenchymal cells, as in the vertebrate neural crest; or (3) dynamic clusters of adherent cells, as in the *Drosophila* border cells (Bianco et al., 2007; Haas and Gilmour, 2006; Mayor and Carmona-Fontaine, 2010; Montell et al., 2012). These cell collectives polarize and migrate by integrating both instructive and permissive cues from their environment. As the immediate environment and cell states change during migration, systematic analyses are required to dissect the relative contributions of intrinsic properties and extrinsic cues to collective polarity and directed migration.

The ascidian *Ciona intestinalis* is a simple and amenable chordate model system with which to study collective cell migration (Beh et al., 2007; Christiaen et al., 2008; Davidson et al., 2005). In *Ciona*, bilateral pairs of cardiac progenitor cells undergo arguably the simplest collective migration. They maintain conspicuous leader-trailer (LT) polarity. The leader forms more prominent protrusions than the trailer, which abuts it and has a constricted trailing end (supplementary material Movie 1; Christiaen et al., 2008). Additionally, TVCs maintain cadherin-based cell-cell adhesion throughout migration (Norton et al., 2013). The *Ciona* cardiogenic lineage arises from a single pair of blastomeres called B7.5, which divide twice during gastrulation, giving rise to pairs of smaller anterior cardiogenic progenitors (trunk ventral cells, TVCs) and larger posterior anterior tail muscles (ATMs; supplementary material Fig. S1; Davidson and Levine, 2003; Satou et al., 2004). The TVCs migrate away from the ATMs towards the ventral trunk, where they subsequently divide asymmetrically, producing distinct heart and the atrial siphon muscle precursors (Davidson and Levine, 2003; Davidson et al., 2005; Stolfi et al., 2010; Wang et al., 2013).

Here, we quantified the contacts between the TVCs and each neighboring tissue, and assayed their role(s) in regulating TVC specification and collective behavior via tissue-specific inhibition of the secretory pathway. Our studies revealed that a combination of extrinsic cues is involved in regulating TVC polarity and guiding their migration. Altering tissue-specific secretion revealed the range of migratory capabilities of TVCs, which surrounding tissues appear primarily to constrain.

RESULTS

Tissue-specific inhibition of the secretory pathway

To broadly evaluate the influence of tissues surrounding the TVCs, we blocked secretion in a tissue-specific manner and assayed TVC polarity and migration. We inhibited the secretory pathway by expressing a dominant-negative form of *Ciona intestinalis* Sar1 (dnSar1), a small GTPase required for vesicle transport from the endoplasmic reticulum (ER) to the Golgi apparatus (Nakano and

Center for Developmental Genetics, Department of Biology, New York University, NY 10003, USA.
*Present address: Skirball Institute of Biomolecular Medicine, NYU School of Medicine, New York, NY 10016, USA.

‡Author for correspondence (lc121@nyu.edu)

Received 21 July 2014; Accepted 1 December 2014

Development (2015) 142, 544-554 doi:10.1242/dev.115444

Muramatsu, 1989; Sato and Nakano, 2007). We created dnSar1 by mutating the threonine (T) at position 35 into an asparagine (N), which locks Sar1 in an inactive GDP-bound state. This inhibits ER-to-Golgi transport of transmembrane proteins, resulting in their accumulation in the ER (Kuge et al., 1994; Quintero et al., 2010). We expect secretory pathway inhibition to affect a range of processes, including cell-cell signaling, deposition of extracellular matrix components and the mechanical properties of the tissue. Although we cannot formally distinguish between these possibilities, we recognize that all of these are likely influenced by dnSar1 expression and would potentially impact TVC migration.

To confirm that dnSar1 inhibits the secretory pathway, we co-electroporated constructs encoding transmembrane glycoproteins: either the vesicular stomatitis virus G fused to GFP (VSVG::GFP; Presley et al., 1997) or human CD4 fused to mCherry (hCD4::mCherry), both of which are normally trafficked through the secretory pathway and localize to the plasma membrane (Fig. 1A,A′; supplementary material Fig. S2A). We used a *FoxF* epidermal enhancer to express VSVG::GFP [FoxF(-845/-1); Fig. 1A-C′; Beh et al., 2007]. As a positive control, we treated embryos with the drug brefeldin A, which inhibits the secretory pathway by preventing ER homeostasis (Klausner et al., 1992). In these embryos, GFP localized to the perinuclear and cytoplasmic space, indicating accumulation in the ER (Fig. 1B,B′). Although control cells formed a compact epithelium, brefeldin A-treated cells were more spherical, consistent with loss of surface adhesion molecules (Fig. 1A-B′). In epidermal cells co-expressing dnSar1, the rounded cell morphology and ER-like accumulation of VSVG::GFP resembled that observed with brefeldin A and published effects of dnSar1 in cultured cells (Fig. 1C,C′; Quintero et al., 2010).

To confirm that dnSar1 expression caused ER accumulation of secreted proteins, we used the ER marker KDELR::GFP (Oda-Ishii and Di Gregorio, 2007). We observed extensive colocalization of KDELR::GFP and hCD4::mCherry in each tissue only when co-expressed with dnSar1 (supplementary material Fig. S2), indicating that *Ciona* dnSar1 inhibits secretion.

To determine whether expression of dnSar1 affected cell survival, we processed control and dnSar1-expressing embryos for TUNEL staining. Embryos were fixed mid-TVC migration (10.5 h post fertilization, hpf; Hotta et al., 2007) and after hatching (24.5 hpf). No positive TUNEL staining in any condition was visible at 10.5 hpf (supplementary material Fig. S3A-E′). At 24.5 hpf,

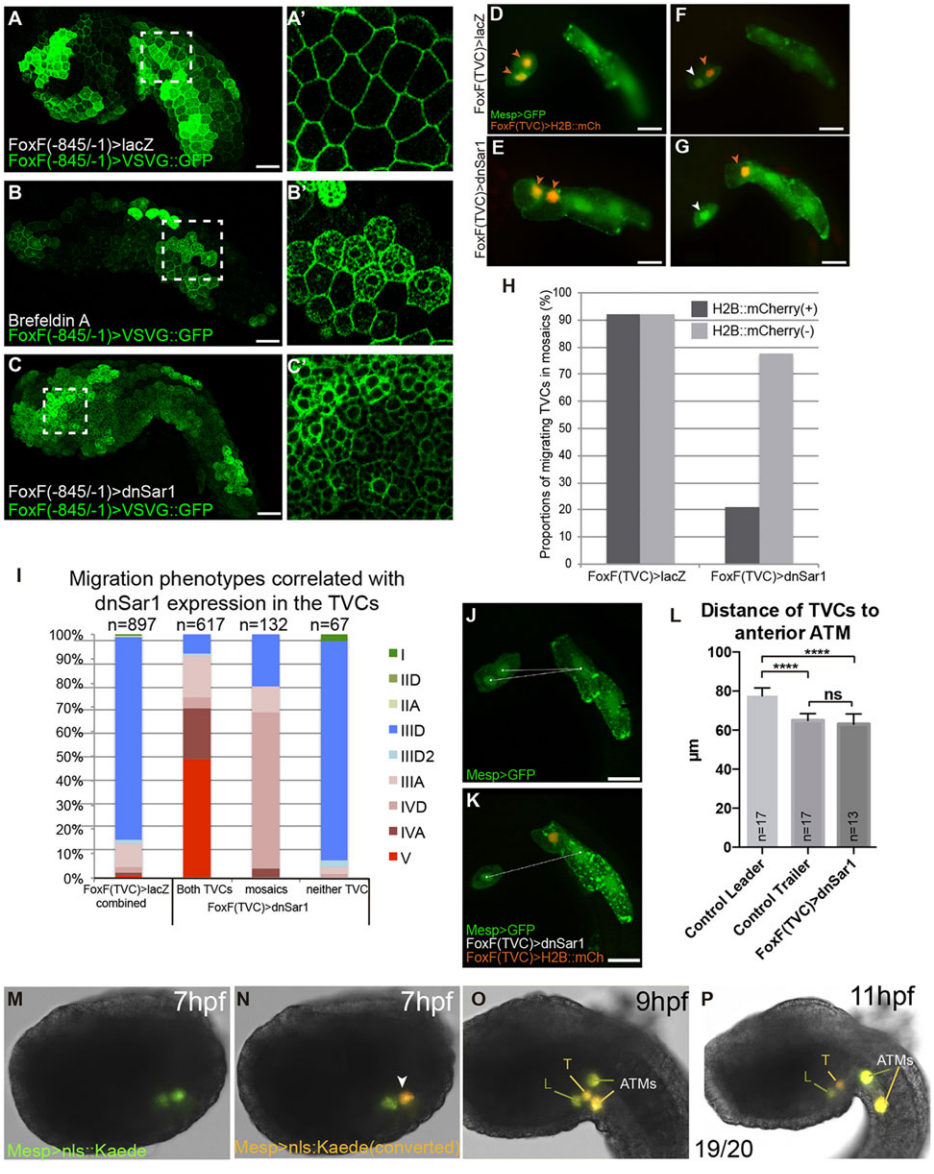

Fig. 1. Mosaic TVC-specific expression of dnSar1 reveals the individual potential of TVCs. Images are of lateral views with anterior towards the left in this and all subsequent figures unless otherwise specified. (A-C′) Embryos electroporated with *FoxF(-845/-1)>VSVG::GFP* (green) and indicated constructs or treatments. (A′-C′) Partial *z*-projections represent boxed regions. (D-G,J,K) Embryos electroporated with *Mesp>GFP* (green), *FoxF(TVC)>H2B::mCherry* (red) and *FoxF(TVC)>lacZ* or *FoxF(TVC)>dnSar1*, as indicated. (D-G) Red arrowheads, H2B::mCherry(+); white arrowheads, H2B::mCherry(–). (H) Proportions of migratory TVCs that are H2B::mCherry (+) or (–), as in indicated conditions. (I) Proportions of migration phenotypes correlated with LT-mosaic expression of H2B::mCherry, as indicated. *n*, number of embryo halves scored. (J,K) White lines: distances measured in Imaris. (L) Average distance between indicated TVCs and anterior ATM. Lines above bars: 95% confidence interval. (M-P) Snapshots at indicated time points. (M,N)Ventral views. n.s., not significant; ****P<0.0001, one-way ANOVA followed by Tukey's multiple comparison test. Scale bars: 25 μm.

Development (2015) 142, 544-554 doi:10.1242/dev.115444

positive TUNEL staining was seen in the retracting posterior larval tail, and in scattered cells throughout the trunk, as previously shown for metamorphosing larvae (supplementary material Fig. S3F-J; Chambon et al., 2002; Tarallo and Sordino, 2004). Aside from these characterized regions of apoptosis, no obvious cell death occurred in any of the tissues expressing dnSar1 (supplementary material Fig. S3F-J′). This shows that dnSar1-expressing cells survive long after TVC migration. We concluded that effects of dnSar1 observed were not caused by toxic cell necrosis, but rather by impacting physiological requirements for each tissue.

We used the *Mesp* enhancer to co-express dnSar1 and hCD4::mCherry in the B7.5 lineage. In all *Mesp>dnSar1*-expressing embryos halves, the 'TVCs' failed to migrate (supplementary material Fig. S4B,C). The TVCs are normally induced by a FGF signal secreted by tissues surrounding the founder cells (Cooley et al., 2011; Davidson et al., 2006). We expected dnSar1 to alter trafficking of the FGF receptor and inhibit TVC specification. To assay FGFR trafficking, we co-electroporated *Mesp>KDELR::GFP* and *Mesp>FGFR::mCherry*. In control embryos, FGFR::mCherry formed discrete puncta distinct from KDELR::GFP expression in the ER (supplementary material Fig. S4D-D‴,F,G). When co-expressed with dnSar1, however, FGFR::mCherry extensively co-localized with KDELR::GFP, confirming its accumulation in the ER (supplementary material Fig. S4E-E‴,F,G).

To test whether dnSar1 expression blocked TVC specification, we used fluorescence *in situ* hybridization (FISH) to assay expression of the TVC and tail muscle markers *Hand-r* (*Hand-related*, renamed after *Hand-like/Notrlc*; Stolfi et al., 2014) and *Myosin regulatory light chain 2* (*Mrlc2*), respectively (Davidson and Levine, 2003; Satou et al., 2004). In contrast to control embryos, where *Hand-r* was expressed in both TVCs, high proportions of *Mesp>dnSar1*-electroporated embryos failed to activate *Hand-r* and repress *Mrlc2* in the smaller B7.5-derived cells (supplementary material Fig. S4H-J). These observations indicate that B7.5-specific inhibition of the secretory pathway blocks TVC specification, contributing to their failure to migrate.

TVCs have equivalent potential to migrate individually and leader-trailer polarity is predetermined

We next assayed the effect of blocking the secretory pathway in the TVCs by expressing dnSar1 using the *FoxF* minimal TVC enhancer (*FoxF(TVC)*), which is activated specifically in the newborn TVCs (Beh et al., 2007). We co-electroporated *Mesp>GFP* and *FoxF(TVC)>H2B::mCherry* with either *FoxF(TVC)>dnSar1* or *FoxF(TVC)>lacZ* and assayed TVC migration, using H2B::mCherry fluorescence as a proxy for *FoxF(TVC)* activity and dnSar1 expression (Fig. 1D-G; Stolfi and Christiaen, 2012). In most *FoxF(TVC)>dnSar1* electroporated embryos, both TVCs expressed H2B::mCherry and showed inhibited TVC migration compared with controls, indicating that dnSar1-mediated inhibition of the secretory pathway blocks migration beyond TVC induction (Fig. 1D,E,H).

About 20% of the Mesp>GFP-positive TVC pairs expressed *FoxF*-driven H2B::mCherry in only one of the two cells (Fig. 1F-I). This variable leader-trailer (LT) mosaicism depends upon electroporation efficacy and reflects unequal plasmid inheritance during divisions, prior to *FoxF* activation (Stolfi and Christiaen, 2012). LT mosaicism allowed us to study the reciprocal effects of TVCs during migration. In control LT-mosaic embryos, the distribution of leader- versus trailer-only expression was not significantly different from 50:50, as expected if plasmids segregate randomly to either cell after the B7.5 division (n=109/211 leader only versus n=102/211 trailer only; χ^2 test, P=0.63; Fig. 1F). By contrast, 91% of LT-mosaic *FoxF(TVC)>dnSar1* embryos showed stronger or exclusive H2B::mCherry expression in the posterior-most TVC, indicating that the dnSar1-negative TVC migrated ahead of its secretion-inhibited cousin cell (Fig. 1G; n=120/132 versus n=12/132; χ^2 test, P=5.4×10^{-21}). Furthermore, 92% of H2B::mCherry(+) cells migrated in control LT mosaics compared with 21% in *FoxF(TVC)>dnSar1* LT-mosaics (n=194/211 versus n=28/132; Fig. 1H). The majority of dnSar1-expressing TVCs remained in the tail, whereas the H2B::mCherry(−) TVC migrated into the trunk (64%, n=85/132, IVD phenotype; Fig. 1I). Further quantifications indicated that individual TVCs migrated a significantly shorter distance than control leader TVCs (P<0.001; Tukey's multiple comparisons test; Fig. 1J-L). As both TVCs have equal chances of inheriting the transgene in LT-mosaic TVCs, these data indicate that, regardless of which cell expresses dnSar1 and fails to migrate, the other 'wild-type' TVC is capable of migrating alone, although imperfectly. These results reveal individual TVCs have equivalent potential to migrate and are capable of migrating in the absence of their cousin partner.

As TVCs are equally motile and associate before migrating but eventually form a polarized pair, we asked whether they have equivalent chances of becoming either the leader or trailer. We photoconverted a nuclear version of Kaede (Razy-Krajka et al., 2014) in the founder cells to test whether their initial arrangement prefigures leader versus trailer selection (Fig. 1M,N). The anterior B8.9 founder cell gave birth to the prospective leader TVC in 95% of the embryos, which is markedly higher than expected upon random leader versus trailer specification (Fisher's exact test, P=3.3×10^{-3}; n=19/20; Fig. 1M-P). These results indicate that, even though TVCs have equivalent migratory capabilities, early positional constraints bias the establishment of leader-trailer polarity.

Individual TVCs can migrate when their cousin TVC is stalled by dnSar1 expression and leader-trailer mosaic distribution of transgenes is random. Thus, the strong positional bias implies that, when the anteroventral prospective leader expresses dnSar1, its cousin TVC passes the stalled cell to migrate individually. We observed this configuration using live imaging of a *FoxF(TVC)>dnSar1* LT-mosaic embryo (supplementary material Movie 2). These data also imply that the leader TVC somehow 'tames' its cousin cell into becoming a following trailer cell as altering signaling from the leader unleashes the migratory potential of the prospective trailer.

Variable early TVC positioning indicated that the cells communicate to associate prior to migration. We evaluated the reproducibility of the relative positions of early TVCs and ATMs in embryos expressing *Mesp>GFP* and *Mesp>H2B::mCherry*. 80% of the newborn TVCs were in direct contact with one another (supplementary material Fig. S5A,G), whereas 20% were initially apart (supplementary material Fig. S5B,C,G). We observed a similar proportion of separated early TVCs marked by *Hand-r* expression (22.6%; χ^2 test P=0.54; supplementary material Fig. S5D-G). The greater proportion of initially disjointed TVCs compared with those that fail to migrate as a pair in control embryos (e.g. Fig. 1I; supplementary material Fig. S5G) indicates that separated TVCs eventually associate and migrate together. Live confocal imaging documented this phenomenon. When TVCs were born apart, the prospective trailer migrated towards the stalled leader before the paired TVCs migrated normally into the ventral trunk (supplementary material Movie 3). These data suggest that TVCs actively communicate to establish cell-cell contact prior to migration.

Development (2015) 142, 544-554 doi:10.1242/dev.115444

The mesenchyme confers robust TVC specification

We visualized and quantified the fraction of the surface of TVCs contacting the mesenchyme from 9 to 12 hpf. We labeled early TVCs using *FoxF(TVC)>2XGFP* and the mesenchyme with hCD4::mCherry driven by the *Twist-like1* enhancer (*Twist>hCD4::mCherry*; Abitua et al., 2012). The proportion of the surface of the TVCs contacting the mesenchyme decreased over the course of migration; on average representing 34.7%, 26.6% and 4.7% of the surface of the TVCs at 9, 10 and 12 hpf, respectively, and transitioned from the anterior to lateral surface of the TVCs (Fig. 2A-E). By 12 hpf, this lateral contact was variable and sometimes completely lost (Fig. 2D,E; supplementary material Fig. S6A,C′). Notably, contacts were more extensive with the trailer than the leader throughout migration, thus indicating a possible source of leader-trailer polarity (Fig. 2C,C′).

To test whether the mesenchyme contributes to TVC specification and migration, we used the *Twist-like1* enhancer to express dnSar1 (Fig. 2G,I,J; supplementary material Fig. S6H,I). Expression of *Twist>dnSar1* caused accumulation of *Twist*-driven hCD4::mCherry in the ER (supplementary material Fig. S2C-D‴), as well as mislocalization of the mesenchyme to the tail (Fig. 2G,I; supplementary material Fig. S6G-I). *Twist>dnSar1* inhibited TVC migration in 52% of embryos compared with 10.5% in *Twist>lacZ*-expressing control embryos (Fig. 2G-J; supplementary material Fig. S6G-I). Specifically, in 23% of the embryo halves scored, only one TVC migrated into the trunk while the other remained in the tail and was often morphologically indistinguishable from the other ATMs (IVD phenotype, *n*=144/624; Fig. 2G,H). The remaining migration-inhibited phenotypes ranged from severe (V) to relatively mild (IIID2; Fig. 2H).

To determine whether lone TVCs migrated as far as paired TVCs in control and *Twist>dnSar1* embryos, we quantified the distance of single versus paired migrating TVCs to the anterior-most ATM (Fig. 2G,I-K). First, leader TVCs migrated a significantly greater distance in control than in *Twist>dnSar1* embryos ($P<0.01$ Tukey's multiple comparisons test; Fig. 2F,I,K), suggesting that the mesenchyme exerts a mild but significant effect on paired TVC migration. Second, single TVCs migrated as well as trailers in control and *Twist>dnSar1* conditions (Fig. 2G,I-K). These data suggest that single TVCs migrate as well as trailer TVCs independently of the mesenchyme.

We then asked whether migration-inhibited TVCs were mis-specified by assaying expression of *Hand-r* and *Mrlc2* in control and Twist>dnSar1-expressing embryos fixed at 8.5, 10 and 12 hpf (Fig. 3A-C′). Unlike ATMs and other tail muscle cells, control TVCs progressively lost *Mrlc2* expression (Fig. 3C-D). The proportion of *Twist>dnSar1*-expressing embryos showing one *Mrlc2*(+) TVC at 12 hpf was similar to that showing the class IVD phenotype, where only one TVC migrated (22% versus 23%; compare Fig. 2H with Fig. 3D). We interpret the TVC-specific decrease of *Mrlc2* expression over time as progressive clearance of *Mrlc2* transcripts inherited from the founder cells. We conclude that TVCs still expressing *Mrlc2* at 12 hpf in the *Twist>dnSar1* embryos, are mis-specified as tail muscles.

Hand-r was expressed in both control TVCs across all stages (96%, *n*=348/363; Fig. 3A,B,C,D). In the *Twist>dnSar1* condition, 24%, 14% and 20% of the 8.5, 10 and 12 hpf embryo halves, respectively,

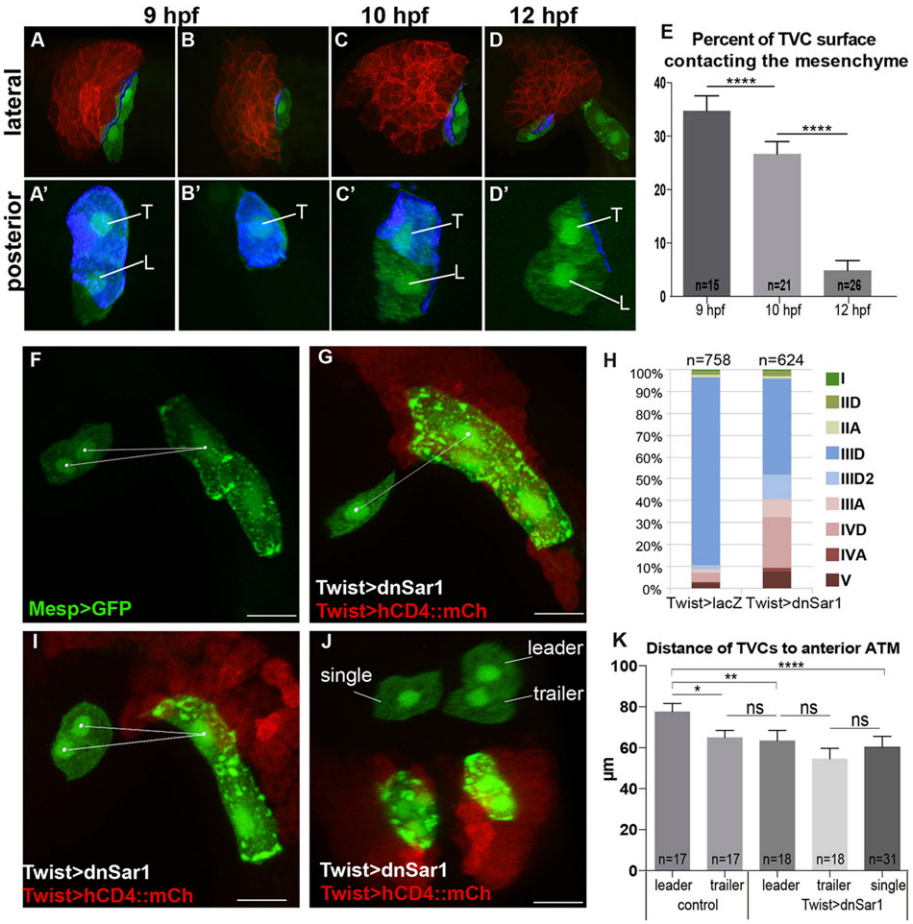

Fig. 2. The mesenchyme makes early extensive contact with the TVCs. (A-D′) Embryos electroporated with *Twist>hCD4::mCherry* (red) and *Mesp>GFP* (green). Blue: area of surface contact between TVCs and mesenchyme. (E) Average percentage of the TVC surface in contact with the mesenchyme at indicated stages. Lines above bars: 95% confidence interval. (F,G,I,J) Embryos electroporated with *Mesp>GFP* (green), *Twist>hCD4::mCherry* (red) and *Twist>dnSar1*. White lines: distance from TVCs to anterior ATM. (J) Ventral view. (H) Proportions of TVC migration phenotypes in indicated conditions. *n*, number of embryo halves scored. (K) Average distance of indicated TVCs from the anterior-most ATM. Lines above bars: 95% confidence interval. n.s., not significant; **P*<0.05, ***P*<0.01, ****P*<0.001, *****P*<0.0001, one-way ANOVA followed by Tukey's multiple comparison test. Scale bars: 25 μm.

Development (2015) 142, 544-554 doi:10.1242/dev.115444

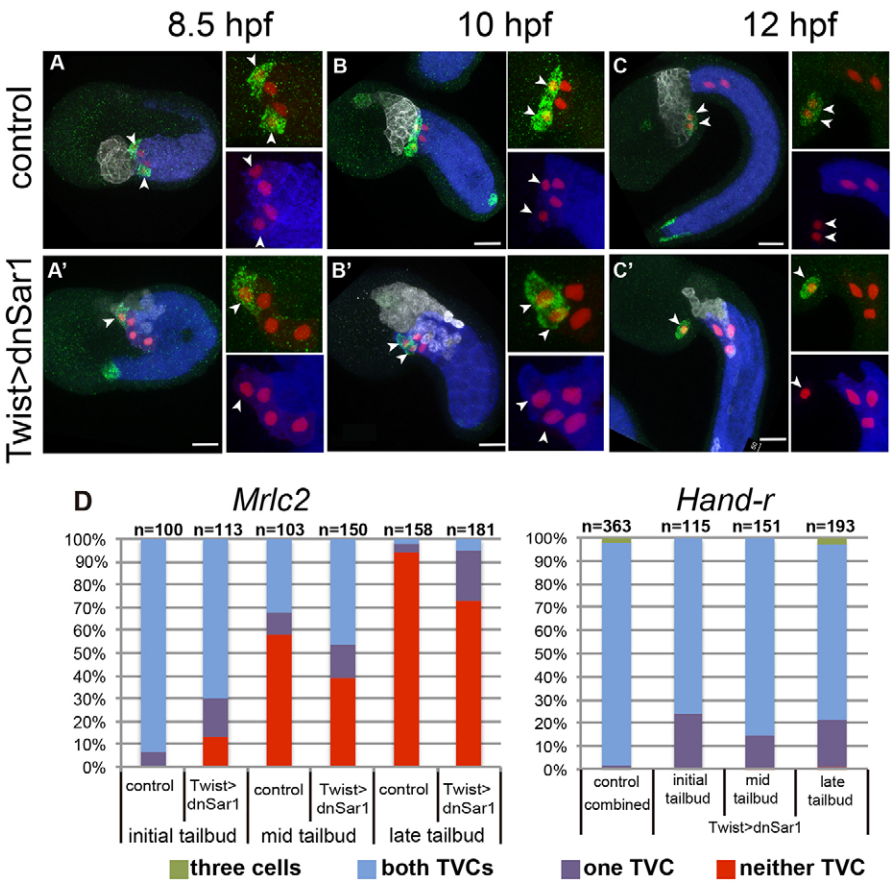

Fig. 3. The mesenchyme contributes to robust specification of the trailer TVC. (A-C′) Embryos electroporated with *Mesp>nls::lacZ* (red), *Twist>hCD4::mCherry* (white) and *Twist>dnSar1* as indicated, showing *Hand-r* (green) and *Mrlc2* (blue) expression. Arrowheads: TVCs. Boxes: *Hand-r* TVC expression. (A,A′) Ventral view. (D) Proportions of embryos expressing either *Mrlc2* or *Hand-r* in indicated number of cells per embryo half. *n*, number of embryo halves scored. Scale bars: 25 µm.

expressed *Hand-r* in only one TVC, whereas 96% of the remaining embryos expressed *Hand-r* in both TVCs (Fig. 3A′,B′,C′,D). These numbers do not differ significantly between stages (χ^2 test, P=0.09), indicating that *Twist>dnSar1* inhibited initial fate specification in one of the two TVCs in an average of 19.1% of the embryos. Furthermore, in 8.5 hpf *Twist>dnSar1* embryos with only one *Hand-r*(+) TVC, this cell was usually in the presumptive leader position (94.5%; n=35/37; Fig. 3A′), suggesting that the mesenchyme contributes to specifying the prospective trailer TVC, in addition to exerting mild effects on the paired migration of induced TVCs.

Inhibiting secretion in the notochord delays the onset of TVC migration

The TVCs are born in proximity to the notochord and migrate away from it. We tested a role for the notochord in repelling the TVCs from the tail by expressing dnSar1 and hCD4::mCherry using the notochord-specific *Brachyury* enhancer (modified from Corbo et al., 1997). *Bra>dnSar1* affected notochord cell shape and convergent extension in ∼80% of the electroporated embryos (supplementary material Fig. S7A-H). TVCs were specified properly in these embryos, as assayed by *Hand-r* and *Mrlc2* expression (supplementary material Fig. S7C,D). We assayed correlated notochord/tail and TVC migration defects in *Bra>LacZ*- or *Bra>dnSar1*-expressing embryos. TVC migration was inhibited in 55.5% of embryos with shortened tails (supplementary material Fig. S7F-H). Sixty-five percent of these embryos displayed the subtle IIID2 phenotype, in which the TVCs were significantly closer to the ATMs than in IIID embryos (supplementary material Fig. S7F,H-L). In *Bra>dnSar1* embryos with shortened tails cultured until 15 hpf, the TVCs reached the ventral trunk and divided as in controls (supplementary material Fig. S7M-O). This suggests that initial migration delays are compensated for by this time.

The endoderm influences the collective polarity and ventral migration of TVCs

To quantify the percentage of the TVC surface in contact with the endoderm before, during and after migration, we expressed hCD4::mCherry throughout the endoderm using the *Nkx2-1* enhancer (formerly called *Ttf1*; modified from Ristoratore et al., 1999) and GFP exclusively in the TVCs using *FoxF(TVC)>2XGFP*. The percentage of the TVC surface area in contact with the endoderm increased over the course of TVC migration; on average, the endoderm contacted 16%, 24% and 49% of the surface of the TVCs at 9, 10 and 12 hpf, respectively (Fig. 4A-C′,E). In 9 hpf embryos, only the median-ventral TVC (the presumptive leader) contacts the *Gata4/Gata5/Gata6*-expressing trunk endoderm [Fig. 4A,A′; *Gata4/Gata5/Gata6* (*Gata4/5/6*) is renamed after *GATAa*; Ragkousi et al., 2011; Stolfi et al., 2014]. By 10 hpf, the anterior and medial surfaces of the leading TVC and a region of the medial surface of the trailer contact the endoderm, appearing as though the TVCs are carving a path through the endoderm (Fig. 4B,B′; supplementary material Fig. S8A). By 12 hpf, the TVCs are tightly apposed to the endoderm along their dorsal surface, residing in endodermal pockets (Fig. 4C,C′; supplementary material Fig. S8B-D; Nakamura et al., 2012).

We used the *Nkx2-1* enhancer to drive dnSar1 and hCD4::mCherry expression in the endoderm and assayed the effects on TVC migration. Previous alteration of endoderm development using a *Nkx2-1*-driven dominant-negative form of *Gata4/5/6* perturbed posterior trunk endoderm morphology and caused a cardia bifida-like phenotype without altering TVC specification or

Development (2015) 142, 544-554 doi:10.1242/dev.115444

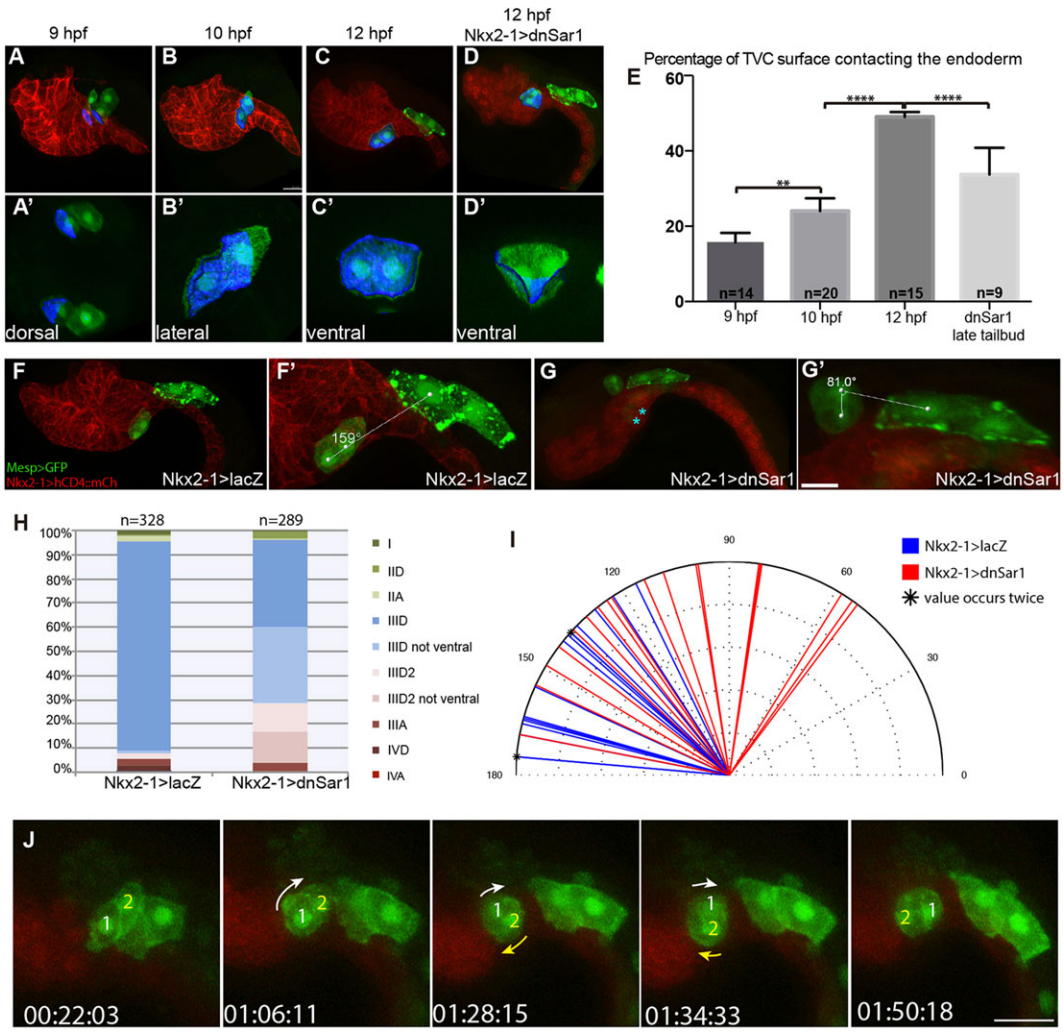

Fig. 4. The endoderm maintains leader-trailer polarity and directs the TVCs ventrally. (A-D′) Embryos electroporated with *Mesp>GFP* (green), *Nkx2-1>hCD4::mCherry* (red) and *Nkx2-1>dnSar1*, as indicated. Blue: area of surface contact between the endoderm and TVCs. (A′-D′) Alternate views of TVCs and area of surface contact from corresponding embryos. (E) Average percentage of TVC surface contacting the endoderm. Lines above bars: 95% confidence interval. ***P*<0.01, *****P*<0.0001, one-way ANOVA followed by Tukey's multiple comparison test. (F-G′) Embryos electroporated with *Mesp>GFP* (green), *Nkx2-1>hCD4::mCherry* (red) and *Nkx2-1>lacZ* or *Nkx2-1>dnSar1*. (F′,G′) Higher magnification of TVCs showing the angle between the leader-trailer and the trailer-anterior ATM axes. Blue asterisks in G indicate expected position of TVCs in normal migration. (H) Proportions of migration phenotypes. *n*, number of electroporated embryo halves scored. (I) Modified rose plot showing angles as measured in Nkx2-1>lacZ and Nkx2-1>dnSar1 electroporated embryos. (J) Selected snapshots from time-lapse of an embryo electroporated with *Mesp>GFP* (green), *Nkx2-1>hCD4::mCherry* (red) and *Nkx2-1>dnSar1*. '1' and '2' represent the same TVCs throughout the time-lapse. White and yellow arrows indicate the directions migrated by TVC 1 and TVC 2 between time points. Scale bars: 25 µm.

forward migration (Ragkousi et al., 2011). Endoderm-specific inhibition of the secretory pathway caused subtle endodermal defects but did not prevent tailbud formation, similar to endoderm ablation (Fig. 4G; Munro and Odell, 2002). Furthermore, the TVCs were specified normally in *Nkx2-1>dnSar1* embryos, as assayed by *Hand-r* and *Mrlc2* expression (supplementary material Fig. S8H-I′). These data confirmed previous observations indicating that signaling from the endoderm is not required for TVC specification (Ragkousi et al., 2011).

Initial TVC positioning at 8.5 hpf was indistinguishable between *Nkx2-1>lacZ*- and *Nkx2-1>dnSar1*-expressing embryos (supplementary material Fig. S8E,E′). However, by the start of migration in *Nkx2-1>dnSar1*-expressing embryos, the TVCs assumed variable positions, some apparently avoiding the endoderm rather than migrating towards it, as in controls (supplementary material Fig. S8F,F′). We observed two major types of TVC migration defects in *Nkx2-1>dnSar1*-expressing embryos. The TVCs migrated anteriorly but to a more laterodorsal location in 44.3% of the embryo halves scored compared with ∼1% in controls (Fig. 4F-H; supplementary material Fig. S8G,G′). In about one quarter of the *Nkx2-1>dnSar1* embryos, TVCs had detached from the ATMs but failed to migrate as far as in controls (class IIID2; 24.9%, *n*=72/289; Fig. 4G-H). These 'short distance' and 'forward-but-not-ventral' migration phenotypes were not mutually exclusive: TVCs migrated neither ventrally nor as far as in controls in 12.8% of the *TTF1>dnSar1* embryos (*n*=37/289; Fig. 4G-H). The percentage of the TVC surface in contact with the endoderm was significantly reduced in 12 hpf *Nkx2-1>dnSar1* embryos (*P*<0.001 Tukey's multiple comparisons test; Fig. 4C-E). These results indicate that a healthy secreting endoderm is required to direct the TVCs ventrally, but not for the TVCs to detach from the muscles and migrate into the trunk.

The TVCs also displayed a remarkable collective polarity phenotype in the *Nkx2-1>dnSar1* electroporated embryos, often

Development (2015) 142, 544-554 doi:10.1242/dev.115444

aligning along the dorsoventral axis despite having migrated anteriorly (Fig. 4F-G′). In control embryos, the LT axis of the TVCs generally aligns with the direction of migration defined by the trailer-ATM axis, forming an average angle of 149° (minimum angle=116°, maximum angle=175°, coefficient of variation=12.65%, *n*=17; Fig. 4F,F′,I). By contrast, in *Nkx2-1>dnSar1* embryos, the orientation of TVCs was more variable relative to the direction of migration; the LT axis forming an average angle of 110° with the trailer-ATM axis (minimum angle=53°, maximum angle=169°, coefficient of variation=31.6%, *n*=19; Fig. 4G,G′,I). Additionally, the TVCs in *Nkx2-1>dnSar1* embryos were often more rounded than in controls (Fig. 4F-G′).

Time-lapse imaging of *Nkx2-1>dnSar1* electroporated embryos clarified the phenotypes observed in fixed samples. In five out of the 13 embryos, the TVCs tumbled at the initiation of migration or after detaching from the ATMs (Fig. 4J; supplementary material Fig. S8J, Movies 4 and 5). In four other cases, the association between the TVCs was dynamic despite incomplete tumbling, and the remaining four cases showed either abnormal migration or unclear TVC relations. Therefore, the increased variability in the angle between the TVCs and their direction of migration reflects active switching of the leader and trailer positions, while the two cells remained adherent. Furthermore, in seven out of 11 time-lapse recordings where the endoderm was well labeled, the TVCs appeared to avoid the affected endoderm and instead migrated dorsally.

Taken together, these observations suggest that dnSar1-inhibited endoderm cells fail to 'attract' the TVCs ventrally and/or constitute physical obstacles to their migration. Alternative possibilities include loss of migratory substrate provided by the endoderm, such as extracellular matrix components whose secretion should be inhibited by dnSar1 expression, and/or changes in stiffness of the endodermal tissue. Our observations also indicate that the endoderm contributes to stabilizing leader-trailer polarity, the plasticity of which was revealed by the tumbling phenotype observed upon *Nkx2-1>dnSar1* expression.

Secretion from the epidermis is required for TVC-TVC adhesion and for ventral migration

The TVCs are born contacting the ventral epidermis (Nishida, 1987; Nishida and Satoh, 1985) and establish integrin-mediated adhesion to the epidermal extracellular matrix, which is required for TVC specification by polarizing sustained MAPK activity (Cooley et al., 2011; Norton et al., 2013). During their migration, TVCs maintain contact with the posterior trunk epidermis (Nishida, 1987; Nishida and Satoh, 1985). To quantify the percentage of the TVC surface in contact with the epidermis before, during and after migration, we expressed hCD4::mCherry using the upstream cis-regulatory DNA of *EphrinB*, which is predominantly expressed in tail and anterior ventral head epidermis (Imai et al., 2004). The *EphrinB* enhancer is active throughout trunk and tail epidermis as well as in a-line (anterior animal lineage) neural cells, which share a common origin with the anterior epidermis (Fig. 5A-C; Nishida, 1987; Nishida and Satoh, 1985). Quantifications showed that the percentage of the TVC surface in contact with the epidermis increases over the course of TVC migration. On average, 24%, 36% and 43% of the TVC surface contacts the epidermis at 9, 10 and 12 hpf, respectively (*n*=8, 16 and 15; Fig. 5A-C′,E). During migration, the TVC-epidermis contact transitions from the lateral to ventral surface of the TVCs as they complete migration flattened in between the trunk endoderm and the ventral epidermis.

We used the *EphrinB* enhancer to express dnSar1 and test a role for the epidermis in TVC migration and/or polarity. In stage 14 control embryos, *EphrinB*-driven hCD4::mCherry localized to the plasma membrane throughout the epidermis, including the b-line cells overlaying the founder cells (supplementary material Fig. S9A; Cooley et al., 2011). In embryos co-electroporated with *EphrinB>dnSar1*, hCD4::mCherry accumulated in an expanded ER and the cells took on a rounded and loosely adherent morphology indicating that *EphrinB>dnSar1* impaired the secretory pathway in the epidermis prior to the birth of the TVCs (supplementary material Fig. S2H-H‴ and Fig. S9A′). Subsequent division of the founder cells during TVC formation in *EphrinB>dnSar1* embryos appeared normal (supplementary material Fig. S9B-C′). However, highly efficient transfections severely disrupted embryonic and B7.5 lineage development, preventing us from interpreting TVC specification and migration phenotypes. These embryos were excluded from subsequent analyses.

We assayed *Hand-r* and *Mrlc2* expression to test whether TVCs were properly specified upon *EphrinB>dnSar1* electroporation. *Hand-r* was expressed in both TVCs in 96% of controls and 85% of *EphrinB>dnSar1* embryos (supplementary material Fig. S9D-F). The TVCs expressed variable levels of *Mrlc2*, whereas ATMs and other tail muscle cells always expressed high levels of *Mrlc2* in both control and *EphrinB>dnSar1*-expressing embryos (supplementary material Fig. S9D-F). These data suggest that secretion from the epidermis is dispensable for early TVC specification. However, it is possible that the component(s) required for TVC induction is(are) secreted by epidermal cells and deposited in the ECM before *EphrinB>dnSar1* action and/or that low initial levels of *EphrinB>dnSar1* do not affect epidermis-dependent early TVC induction.

The severity of TVC migration phenotypes was correlated with transgene mosaicism in the epidermis as assayed by hCD4::mCherry expression (Fig. 5H). When dnSar1 was expressed throughout the epidermis, the two main observed phenotypes were 'mild inhibition', where TVCs migrated as a pair but not as far as controls (IIID2, 41%; Fig. 5H) and complete inhibition, where both TVCs remained in the tail (V, 25%; Fig. 5H). Specific defects were still observed when only the b-line tail epidermis expressed dnSar1, suggesting early inputs from these cells are required for proper TVC migration in addition to a role for the a-line trunk epidermis.

Standard phenotypic categories did not fully describe our observations. Additional and non-mutually exclusive phenotypes included decreased or complete loss of association between migrating TVCs, which were often more spherical than control TVCs, and 'forward-but-not-ventral' migration (Fig. 5F,G,I,J; supplementary material Fig. S9H-K). When the entire epidermis expressed dnSar1, these non-standard TVC migration phenotypes were observed in 44% of the embryos compared with 42.4% when half the epidermis expressed dnSar1 (supplementary material Fig. S9G). This indicated that these phenotypes are due to secretion inhibition in the a-line head epidermis on the same side as the TVCs. Specifically, TVCs migrated separately in 12.6% and 10.7% of embryo halves when either the entire epidermis or one half of the epidermis expressed dnSar1, respectively (*n*=12/95 versus *n*=17/158). TVCs were loosely associated in 20% (*n*=19/95) and 14.5% (*n*=23/158) of the embryos halves when either all or one half of the epidermis expressed dnSar1, compared with less than 1% (*n*=3/356) in controls. These observations suggest that the same-side a-line head epidermis contributes to the cell-cell adhesion of TVCs and TVC-epidermis adhesion.

The percentages of the TVC surface in contact with the epidermis were measured in *EphrinB>dnSar1* embryos for both singly

Development (2015) 142, 544-554 doi:10.1242/dev.115444

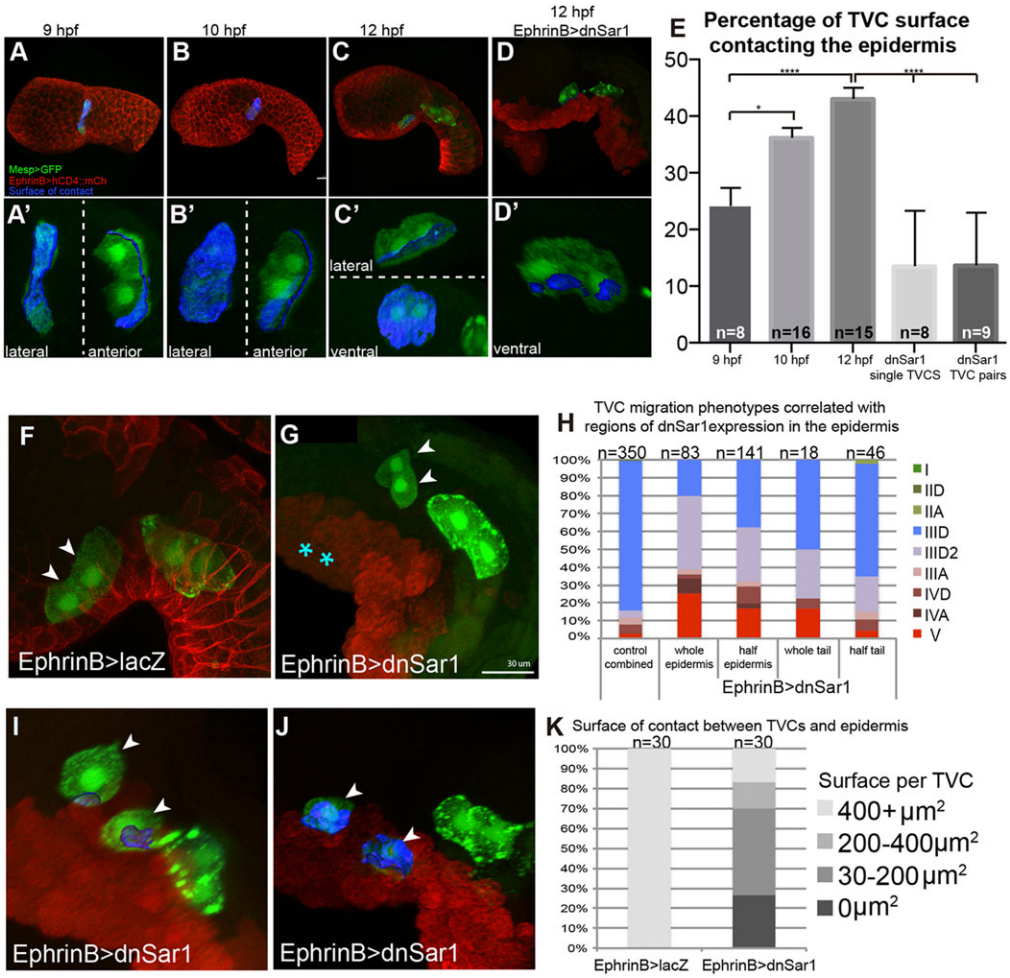

Fig. 5. The epidermis determines TVC-TVC and TVC-ECM adhesions. (A-D) Embryos electroporated with *Mesp>GFP* (green), *EphrinB>hCD4::mCherry* (red) and *EphrinB>dnSar1*, as indicated. Area of surface contact between TVCs and epidermis is in blue. (A′-D′) Higher magnification images of TVCs and area of surface contact. (E) Average percentage of the TVC surface in contact with the epidermis. Lines above bars: 95% confidence interval. (F,G,I,J) Embryos electroporated with *Mesp>GFP* (green), *EphrinB>hCD4::mCherry* (red) and *EphrinB>lacZ* or *EphrinB>dnSar1*. Arrowheads: TVCs. Blue asterisks: expected position of TVCs in normal migration. (I,J) Blue: area of surface contact with the epidermis. (H) Proportions of TVC migration phenotypes categorized based on mosaicism of hCD4::mCherry expression in the epidermis. *n*, number of embryo halves scored. (K) Area of surface contact between the TVCs and the epidermis calculated per TVC. Categories based on thresholds of surface area. Quantifications of paired TVCs were divided by two and therefore counted twice. *n*, number of TVCs. **P*<0.05, *****P*<0.0001, one-way ANOVA followed by Tukey's multiple comparison test.

migrating and paired TVCs. On average ~13.5% of the TVC surface contacted the labeled epidermis in *EphrinB>dnSar1*-expressing embryos, relative to 43% in controls (Fig. 5D-E,G,I,J; supplementary material Fig. S9H-K). These measurements included TVCs that did not contact the labeled epidermis (20%, *n*=8/40, Fig. 5G,K; supplementary material Fig. S9I-K) and those that made very little contact with the epidermis (52.5%, *n*=21/40, Fig. 5I,K; supplementary material Fig. S9H-J, although we can not rule out contact with contralateral unlabeled epidermis in left/right mosaics), whereas all control TVCs extensively contacted the labeled epidermis (*n*=30/30; Fig. 5C,C′,E,K). Therefore, we conclude that secretion from the epidermis is required for flattening of TVCs onto the epidermal basal lamina.

Time-lapse imaging of *EphrinB>dnSar1* electroporated embryos reflected and clarified phenotypes seen in fixed embryos. Epidermal cells were loosely adherent and constantly shifting, with some cells separating from the embryos, further confirming loss of cell-cell adhesion (supplementary material Movies 6 and 7). We observed TVCs that failed to associate and departed from the ATMs at different times and TVCs that migrated along the dorsal midline rather than ventrally (supplementary material Movies 6 and 7). Therefore, despite severe embryonic abnormalities, the TVCs were specified and migratory, albeit displaying characteristic defects including reduced TVC-TVC adhesion and TVC-ECM adhesion with the dnSar1-expressing epidermis. In summary, our data indicate that, in addition to an early function in establishing asymmetrical TVC induction, the a-line trunk epidermis plays roles in maintaining adhesion between the TVCs, and contributes to their attraction and adhesion to the ventral trunk.

DISCUSSION

Ciona cardiopharyngeal progenitors: the simplest possible model for collective migration

Here, we have characterized the cellular context for migration of the ascidian multipotent cardiopharyngeal progenitors, called trunk ventral cells (TVCs). We quantified contacts with surrounding tissues and showed that TVCs are born adhering to the tail epidermis, B-line mesenchyme and their sister ATMs. The TVCs migrate away from these tissues and develop contacts with the trunk endoderm and a-line epidermis. We developed a genetically encoded dominant-negative Sar1 to block the secretory pathway in a tissue-specific manner and probe the contribution of each surrounding tissue to TVC specification, collective polarity and migration. We first showed that, even though TVCs normally form a polarized pair with a predetermined leader and trailer, each cell can migrate without its cousin TVC, but over a shorter distance and with different morphology from paired TVCs. We show that the mesenchyme contributes to robust specification of the trailer TVC but appears to make only a minor contribution to TVC migration. The notochord, which never contacts the TVCs, contributes to the timely onset of TVC migration. The trunk endoderm, which initially contacts the prospective leader TVC, is required for maintenance of leader-trailer polarity and for the ventral migration of TVCs. Finally, adhesion to the epidermis appeared necessary for TVCs to associate

Development (2015) 142, 544-554 doi:10.1242/dev.115444

and move anteriorly. Our data show that the stereotyped polarity and directed migration of motile TVCs is constrained by a combination of cues from diverse tissues. Experimentally releasing the constraints that each of these tissues imposes on the TVCs revealed their wide range of migratory capabilities.

The TVCs are intrinsically motile and competent for directed migration

Previous studies demonstrated that the migratory behavior of TVCs is determined by cell-autonomous transcriptional mechanisms (Beh et al., 2007; Christiaen et al., 2008, 2010; Davidson et al., 2006, 2005; Ragkousi et al., 2011; Satou et al., 2004; reviewed by Tolkin and Christiaen, 2012). Studies indicated that the cardiopharyngeal founder cells are exposed to a uniform distribution of FGF ligands and that TVC induction occurs via asymmetrical integrin-mediated adhesion with the epidermis (Cooley et al., 2011; Norton et al., 2013). These studies indicated that both TVCs are induced by essentially the same mechanism. Unexpectedly, we found that the mesenchyme exerts an asymmetrical role during TVC specification, contributing to robust specification of the trailer but not the leader TVC. This opens the possibility that the trailer depends more on the mesenchyme as a source of FGF ligands for induction. Unequivocal identification of the TVC-inducing FGF ligand(s) will be necessary to formally establish the signaling mechanisms that govern TVC induction.

None of the tested perturbations blocked the motility of TVCs once they were induced. In *Drosophila*, the border cells depend on JAK/STAT signaling both for their specification and maintenance as a migratory population (Silver et al., 2005; Silver and Montell, 2001). This contrasts with the notion that TVC motility is cell-autonomously controlled by transcriptional mechanisms, even though we cannot formally rule out the possibility that an unidentified signal plays an analogous role to that of JAK/STAT in border cells. It is also possible that several surrounding tissues play redundant roles by secreting either the same or related molecules with equivalent motility-inducing effects. Future studies combining dnSar1 expression in multiple tissues will be necessary to address this possibility.

Ciona TVCs are capable of migrating individually towards the trunk, as shown by mosaic expression of *FoxF(TVC)>dnSar1* and in the *Twist>dnSar1* condition. However, our results indicate that single TVCs migrate only as far as trailers and are morphologically distinct from paired TVCs in that they have both a leading and trailing edge while these two features are normally divided between the leader and trailer, respectively. In several other examples of collective migrations, individual cells do not migrate as well as their cohesive counterparts. For example, *Xenopus* neural crest cells need to form clusters of at least two or three cells to respond to chemotactic cues, as individual neural crest cells respond poorly to chemotactic cues and their migration is misdirected (Theveneau et al., 2010). In *Drosophila*, knocking down E-cadherin in the central polar cells causes the border cell clusters to split into smaller groups and single cells, which are still migratory albeit slower than the associated clusters (Denise Montell and Dafeng Cai, personal communication; Cai et al., 2014). Finally, in the zebrafish, single mesendoderm cells were capable of migrating normally, except when cell-cell adhesion was impaired (Arboleda-Estudillo et al., 2010). Thus, even though cell-autonomous intrinsic motility appears to be a rather common property of collectively migrating cells, the TVCs may stand out in their ability to undergo qualitatively the same directed migration, whether alone or as a leader-trailer polarized pair.

TVC-TVC adhesion and TVC-ECM adhesion require signals from the epidermis

Even though TVCs can migrate individually, they normally migrate as polarized pairs and our observations indicate that they actively associate prior to the onset of migration. The *Xenopus* neural crest uses a system of co-attraction to prevent dispersal by expressing both the secreted complement fragment C3a and its receptor C3aR (Carmona-Fontaine et al., 2011). Notably, whole-genome profiling and *in situ* hybridization assays revealed that a complement fragment 6-like gene is expressed in the TVCs (Christiaen et al., 2008). Futures studies will assay whether C6-like plays a role in the early mutual attraction of TVCs.

Once the TVCs associate, they remain adherent throughout migration. In the absence of signaling from the epidermis, the TVCs frequently dissociated from each other and assumed a spherical morphology indicative of detachment from the epidermis. We hypothesize that failure to maintain a functional epidermal extracellular matrix would alter TVC-ECM association and thus may affect cell-cell adhesion. Indeed, TVCs express several cell-cell and cell-ECM adhesion molecules, including cadherins and integrins, which have been shown to crosstalk in other systems where integrin-ECM adhesion promotes cadherin-mediated cell-cell adhesion (Canel et al., 2013; Christiaen et al., 2008; Marsden and DeSimone, 2003; Martinez-Rico et al., 2010; Shewan et al., 2005; Weber et al., 2011; Woznica et al., 2012). Future studies will determine whether the integrins and/or other cell-matrix adhesion systems are involved in cell-cell and cell-matrix adhesions of TVCs during migration.

Extrinsic instructions for the collective polarity of TVCs

The TVCs normally maintain stable leader-trailer polarity that is determined by the relative positions of the founder cells prior to asymmetric divisions. In the absence of signaling from the endoderm, the TVCs dynamically switched positions while maintaining contact with one another. This indicates that leader-trailer polarity is not autonomous to the TVCs and requires signaling from the endoderm for steady-state stabilization. As only the prospective leader TVC initially contacts the endoderm, we hypothesize that this contact specifies the leader state. Once specified, the leader could signal to the trailer, 'taming' it by either inducing a specific trailer state and/or inhibiting it from becoming a leader, as is the case in *Drosophila* border cells where Rac activation in the leader cell inhibits the motility of followers (Bianco et al., 2007; Prasad and Montell, 2007; Wang et al., 2010). In the absence of signaling from the endoderm, perhaps neither the leader nor the trailer are specified or the trailer is not 'tamed', though both are inherently migratory and thus dynamically change positions. Furthermore, in the absence of signaling from the endoderm, the TVCs did not migrate as far as in controls and often went forward but not ventral. The reduced distance migrated could be due in part to the polarity defect; the TVCs spent more of their migratory efforts tumbling rather than migrating collectively in the same direction. Numerous possibilities that are not mutually exclusive could explain this TVC polarity phenotype, including loss or reduction of ECM normally secreted by the endoderm required by the TVCs as a migratory substrate, altered endoderm integrity, such as changes in stiffness and connectivity that affect the way in which the TVCs and endoderm interact, as well as loss of guidance cues normally secreted by the endoderm.

Migrating cells of the zebrafish LLP are similar to the TVCs in that they generally maintain stable positions with fixed leaders (Haas and Gilmour, 2006). Primordia mutant for the chemokine receptor

Development (2015) 142, 544-554 doi:10.1242/dev.115444

Cxcr4b show dynamic tumbling behavior and therefore, similar to the TVCs, display a wide range of migratory capabilities that are normally canalized (Haas and Gilmour, 2006). Recent studies showed that the collective polarity of the LLP also shapes the gradient of the chemoattractant Sdf1 (Dona et al., 2013; Venkiteswaran et al., 2013). As the TVC collective comprises only two cells, it seems unlikely that LT polarity is required to sharpen extracellular cues. Instead, we hypothesize that TVC association is crucial for subsequent cardiopharyngeal development. *Ciona* develops following stereotyped patterns arising from invariant cell lineages, which generally do not compensate for one another (Lemaire, 2009). Future studies will explore the causal relationships between the polarized migration of TVCs, and their subsequent oriented asymmetric cell divisions and fate specification events.

MATERIALS AND METHODS

Embryo preparation, electroporation and pharmacological treatments

Gravid *Ciona intestinalis* adults were purchased from M-Rep. Isolation of gametes, fertilization, dechorionation and electroporations were performed as described previously using 25-75 µg of plasmid DNA per construct (Christiaen et al., 2009a,b; Corbo et al., 1997). All embryonic time points are given in hours post-fertilization for embryos raised at 18°C. Brefeldin A (Invitrogen) was diluted to a final concentration of 2-5 µg/ml and embryos were bathed for 2-3 h.

Molecular cloning

A cDNA fragment corresponding to the *Ciona intestinalis* Sar1-coding sequence was amplified by RT-PCR. Quickchange mutagenesis was used to generate a dominant-negative Sar1. Tissue-specific enhancers were cloned from genomic DNA using standard methods. Primer sequences are listed in supplementary material Table S1.

In situ hybridization and immunohistochemistry

Single and double whole-mount fluorescent *in situ* hybridization and immunohistochemistry were performed as described previously (Wang et al., 2013), using tyramide signal amplification (TSA kits), anti-β-galactosidase monoclonal mouse antibody (Promega, 23781, 1:500), anti-mCherry rabbit polyclonal antibody (Biovision, 5993-100, 1:500), goat anti-mouse secondary antibody conjugated to Alexa-fluor 555 (Invitrogen, A21422, 1:500) and goat anti-rabbit secondary antibody conjugated to Alexa-fluor 594 (Invitrogen, A11012, 1:500).

Confocal imaging, Kaede photoconversion and image analysis

Embryos were imaged using either a Leica TCS SP5 or an inverted TCS SP8 X confocal microscope. Time-lapse imaging was performed on the SP8 X microscope. Image analyses were performed using the Imaris software (Bitplane, X64, 7.6.4). Imaris was used to render surfaces, to assay colocalization, to quantify distances and angles, and to measure the surface area in contact between tissues. Statistical analyses were performed in Excel and GraphPadPrism. Kaede was converted using the 405 nm diode laser of the inverted TCS SP8 X confocal microscope as described previously (Razy-Krajka et al., 2014).

Acknowledgements

We thank the Christiaen lab members for helpful feedback. We thank Alexandro Ramirez for help in generating the modified rose plot.

Competing interests

The authors declare no competing or financial interests.

Author contributions

L.C. and S.G. conceived, designed and performed the experiments. N.K. performed the photoconversion experiments. Y.B. cloned Mesp>FGFR::mCherry and performed early time-lapse imaging. Y.A. cloned FoxF(-845/-1)>VSVG::GFP and FoxF(-845/-1)>lacZ, and helped conceive the experiments. The manuscript was written by L.C. and S.G.

Funding

This work was supported by the National Institutes of Health [1F32GM105216-01A1 to S.G. and NIH/NIGMS R01 GM096032 to L.C.]. Deposited in PMC for release after 12 months.

Supplementary material

Supplementary material available online at
http://dev.biologists.org/lookup/suppl/doi:10.1242/dev.115444/-/DC1

References

Abitua, P. B., Wagner, E., Navarrete, I. A. and Levine, M. (2012). Identification of a rudimentary neural crest in a non-vertebrate chordate. *Nature* **492**, 104-107.

Aman, A. and Piotrowski, T. (2010). Cell migration during morphogenesis. *Dev. Biol.* **341**, 20-33.

Arboleda-Estudillo, Y., Krieg, M., Stühmer, J., Licata, N. A., Muller, D. J. and Heisenberg, C.-P. (2010). Movement directionality in collective migration of germ layer progenitors. *Curr. Biol.* **20**, 161-169.

Beh, J., Shi, W., Levine, M., Davidson, B. and Christiaen, L. (2007). FoxF is essential for FGF-induced migration of heart progenitor cells in the ascidian Ciona intestinalis. *Development* **134**, 3297-3305.

Bianco, A., Poukkula, M., Cliffe, A., Mathieu, J., Luque, C. M., Fulga, T. A. and Rørth, P. (2007). Two distinct modes of guidance signalling during collective migration of border cells. *Nature* **448**, 362-365.

Cai, D., Chen, S.-C., Prasad, M., He, L., Wang, X., Choesmel-Cadamuro, V., Sawyer, J. K., Danuser, G. and Montell, D. J. (2014). Mechanical feedback through e-cadherin promotes direction sensing during collective cell migration. *Cell* **157**, 1146-1159.

Canel, M., Serrels, A., Frame, M. C. and Brunton, V. G. (2013). E-cadherin-integrin crosstalk in cancer invasion and metastasis. *J. Cell Sci.* **126**, 393-401.

Carmona-Fontaine, C., Theveneau, E., Tzekou, A., Tada, M., Woods, M., Page, K. M., Parsons, M., Lambris, J. D. and Mayor, R. (2011). Complement fragment C3a controls mutual cell attraction during collective cell migration. *Dev. Cell* **21**, 1026-1037.

Chambon, J. P., Soule, J., Pomies, P., Fort, P., Sahuquet, A., Alexandre, D., Mangeat, P. H. and Baghdiguian, S. (2002). Tail regression in Ciona intestinalis (Prochordate) involves a Caspase-dependent apoptosis event associated with ERK activation. *Development* **129**, 3105-3114.

Christiaen, L., Davidson, B., Kawashima, T., Powell, W., Nolla, H., Vranizan, K. and Levine, M. (2008). The transcription/migration interface in heart precursors of Ciona intestinalis. *Science* **320**, 1349-1352.

Christiaen, L., Wagner, E., Shi, W. and Levine, M. (2009a). Electroporation of transgenic DNAs in the sea squirt Ciona. *Cold Spring Harb. Protoc.* **2009**, pdb prot5345.

Christiaen, L., Wagner, E., Shi, W. and Levine, M. (2009b). Isolation of sea squirt (Ciona) gametes, fertilization, dechorionation, and development. *Cold Spring Harb. Protoc.* **2009**, ppdb prot5344.

Christiaen, L., Stolfi, A. and Levine, M. (2010). BMP signaling coordinates gene expression and cell migration during precardiac mesoderm development. *Dev. Biol.* **340**, 179-187.

Cooley, J., Whitaker, S., Sweeney, S., Fraser, S. and Davidson, B. (2011). Cytoskeletal polarity mediates localized induction of the heart progenitor lineage. *Nat. Cell Biol.* **13**, 952-957.

Corbo, J. C., Levine, M. and Zeller, R. W. (1997). Characterization of a notochord-specific enhancer from the Brachyury promoter region of the ascidian, Ciona intestinalis. *Development* **124**, 589-602.

Davidson, B. and Levine, M. (2003). Evolutionary origins of the vertebrate heart: specification of the cardiac lineage in Ciona intestinalis. *Proc. Natl. Acad. Sci. USA* **100**, 11469-11473.

Davidson, B., Shi, W. and Levine, M. (2005). Uncoupling heart cell specification and migration in the simple chordate Ciona intestinalis. *Development* **132**, 4811-4818.

Davidson, B., Shi, W., Beh, J., Christiaen, L. and Levine, M. (2006). FGF signaling delineates the cardiac progenitor field in the simple chordate, Ciona intestinalis. *Genes Dev.* **20**, 2728-2738.

Donà, E., Barry, J. D., Valentin, G., Quirin, C., Khmelinskii, A., Kunze, A., Durdu, S., Newton, L. R., Fernandez-Minan, A., Huber, W. et al. (2013). Directional tissue migration through a self-generated chemokine gradient. *Nature* **503**, 285-289.

Friedl, P. and Gilmour, D. (2009). Collective cell migration in morphogenesis, regeneration and cancer. *Nat. Rev. Mol. Cell Biol.* **10**, 445-457.

Haas, P. and Gilmour, D. (2006). Chemokine signaling mediates self-organizing tissue migration in the zebrafish lateral line. *Dev. Cell* **10**, 673-680.

Hotta, K., Mitsuhara, K., Takahashi, H., Inaba, K., Oka, K., Gojobori, T. and Ikeo, K. (2007). A web-based interactive developmental table for the ascidian Ciona

intestinalis, including 3D real-image embryo reconstructions: I. From fertilized egg to hatching larva. *Dev. Dyn.* **236**, 1790-1805.
Imai, K. S., Hino, K., Yagi, K., Satoh, N. and Satou, Y. (2004). Gene expression profiles of transcription factors and signaling molecules in the ascidian embryo: towards a comprehensive understanding of gene networks. *Development* **131**, 4047-4058.
Klausner, R. D., Donaldson, J. G. and Lippincott-Schwartz, J. (1992). Brefeldin A: insights into the control of membrane traffic and organelle structure. *J. Cell Biol.* **116**, 1071-1080.
Kuge, O., Dascher, C., Orci, L., Rowe, T., Amherdt, M., Plutner, H., Ravazzola, M., Tanigawa, G., Rothman, J. E. and Balch, W. E. (1994). Sar1 promotes vesicle budding from the endoplasmic reticulum but not Golgi compartments. *J. Cell Biol.* **125**, 51-65.
Lemaire, P. (2009). Unfolding a chordate developmental program, one cell at a time: invariant cell lineages, short-range inductions and evolutionary plasticity in ascidians. *Dev. Biol.* **332**, 48-60.
Marsden, M. and DeSimone, D. W. (2003). Integrin-ECM interactions regulate cadherin-dependent cell adhesion and are required for convergent extension in Xenopus. *Curr. Biol.* **13**, 1182-1191.
Martinez-Rico, C., Pincet, F., Thiery, J.-P. and Dufour, S. (2010). Integrins stimulate E-cadherin-mediated intercellular adhesion by regulating Src-kinase activation and actomyosin contractility. *J. Cell Sci.* **123**, 712-722.
Mayor, R. and Carmona-Fontaine, C. (2010). Keeping in touch with contact inhibition of locomotion. *Trends Cell Biol.* **20**, 319-328.
Montell, D. J., Yoon, W. H. and Starz-Gaiano, M. (2012). Group choreography: mechanisms orchestrating the collective movement of border cells. *Nat. Rev. Mol. Cell Biol.* **13**, 631-645.
Munro, E. M. and Odell, G. (2002). Morphogenetic pattern formation during ascidian notochord formation is regulative and highly robust. *Development* **129**, 1-12.
Nakamura, M. J., Terai, J., Okubo, R., Hotta, K. and Oka, K. (2012). Three-dimensional anatomy of the Ciona intestinalis tailbud embryo at single-cell resolution. *Dev. Biol.* **372**, 274-284.
Nakano, A. and Muramatsu, M. (1989). A novel Gtp-binding protein, Sar1p, is involved in transport from the endoplasmic-reticulum to the Golgi-apparatus. *J. Cell Biol.* **109**, 2677-2691.
Nishida, H. (1987). Cell lineage analysis in ascidian embryos by intracellular injection of a tracer enzyme. III. Up to the tissue restricted stage. *Dev. Biol.* **121**, 526-541.
Nishida, H. and Satoh, N. (1985). Cell lineage analysis in ascidian embryos by intracellular injection of a tracer enzyme. II. The 16- and 32-cell stages. *Dev. Biol.* **110**, 440-454.
Norton, J., Cooley, J., Islam, A. F. M. T., Cota, C. D. and Davidson, B. (2013). Matrix adhesion polarizes heart progenitor induction in the invertebrate chordate Ciona intestinalis. *Development* **140**, 1301-1311.
Oda-Ishii, I. and Di Gregorio, A. (2007). Lineage-independent mosaic expression and regulation of the Ciona multidom gene in the ancestral notochord. *Dev. Dyn.* **236**, 1806-1819.
Prasad, M. and Montell, D. J. (2007). Cellular and molecular mechanisms of border cell migration analyzed using time-lapse live-cell imaging. *Dev. Cell* **12**, 997-1005.
Presley, J. F., Cole, N. B., Schroer, T. A., Hirschberg, K., Zaal, K. J. and Lippincott-Schwartz, J. (1997). ER-to-Golgi transport visualized in living cells. *Nature* **389**, 81-85.
Quintero, C. A., Giraudo, C. G., Villarreal, M., Montich, G. and Maccioni, H. J. F. (2010). Identification of a site in Sar1 involved in the interaction with the cytoplasmic tail of glycolipid glycosyltransferases. *J. Biol. Chem.* **285**, 30340-30346.
Ragkousi, K., Beh, J., Sweeney, S., Starobinska, E. and Davidson, B. (2011). A single GATA factor plays discrete, lineage specific roles in ascidian heart development. *Dev. Biol.* **352**, 154-163.
Razy-Krajka, F., Lam, K., Wang, W., Stolfi, A., Joly, M., Bonneau, R. and Christiaen, L. (2014). Collier/OLF/EBF-dependent transcriptional dynamics control pharyngeal muscle specification from primed cardiopharyngeal progenitors. *Dev. Cell* **29**, 263-276.
Ristoratore, F., Spagnuolo, A., Aniello, F., Branno, M., Fabbrini, F. and Di Lauro, R. (1999). Expression and functional analysis of Cititf1, an ascidian NK-2 class gene, suggest its role in endoderm development. *Development* **126**, 5149-5159.
Rørth, P. (2012). Fellow travellers: emergent properties of collective cell migration. *EMBO Rep.* **13**, 984-991.
Sato, K. and Nakano, A. (2007). Mechanisms of COPII vesicle formation and protein sorting. *FEBS Lett.* **581**, 2076-2082.
Satou, Y., Imai, K. S. and Satoh, N. (2004). The ascidian Mesp gene specifies heart precursor cells. *Development* **131**, 2533-2541.
Shewan, A. M., Maddugoda, M., Kraemer, A., Stehbens, S. J., Verma, S., Kovacs, E. M. and Yap, A. S. (2005). Myosin 2 is a key Rho kinase target necessary for the local concentration of E-cadherin at cell-cell contacts. *Mol. Biol. Cell* **16**, 4531-4542.
Silver, D. L. and Montell, D. J. (2001). Paracrine signaling through the JAK/STAT pathway activates invasive behavior of ovarian epithelial cells in Drosophila. *Cell* **107**, 831-841.
Silver, D. L., Geisbrecht, E. R. and Montell, D. J. (2005). Requirement for JAK/STAT signaling throughout border cell migration in Drosophila. *Development* **132**, 3483-3492.
Stolfi, A. and Christiaen, L. (2012). Genetic and genomic toolbox of the chordate Ciona intestinalis. *Genetics* **192**, 55-66.
Stolfi, A., Gainous, T. B., Young, J. J., Mori, A., Levine, M. and Christiaen, L. (2010). Early chordate origins of the vertebrate second heart field. *Science* **329**, 565-568.
Stolfi, A., Lowe, E. K., Racioppi, C., Ristoratore, F., Brown, C. T., Swalla, B. J. and Christiaen, L. (2014). Divergent mechanisms regulate conserved cardiopharyngeal development and gene expression in distantly related ascidians. *eLife* **3**, e03728.
Tarallo, R. and Sordino, P. (2004). Time course of programmed cell death in Ciona intestinalis in relation to mitotic activity and MAPK signaling. *Dev. Dyn.* **230**, 251-262.
Theveneau, E., Marchant, L., Kuriyama, S., Gull, M., Moepps, B., Parsons, M. and Mayor, R. (2010). Collective chemotaxis requires contact-dependent cell polarity. *Dev. Cell* **19**, 39-53.
Tolkin, T. and Christiaen, L. (2012). Development and evolution of the ascidian cardiogenic mesoderm. *Curr. Top. Dev. Biol.* **100**, 107-142.
Venkiteswaran, G., Lewellis, S. W., Wang, J., Reynolds, E., Nicholson, C. and Knaut, H. (2013). Generation and dynamics of an endogenous, self-generated signaling gradient across a migrating tissue. *Cell* **155**, 674-687.
Wang, X., He, L., Wu, Y. I., Hahn, K. M. and Montell, D. J. (2010). Light-mediated activation reveals a key role for Rac in collective guidance of cell movement in vivo. *Nat. Cell Biol.* **12**, 591-597.
Wang, W., Razy-Krajka, F., Siu, E., Ketcham, A. and Christiaen, L. (2013). NK4 antagonizes Tbx1/10 to promote cardiac versus pharyngeal muscle fate in the ascidian second heart field. *PLoS Biol.* **11**, e1001725.
Weber, G. F., Bjerke, M. A. and DeSimone, D. W. (2011). Integrins and cadherins join forces to form adhesive networks. *J. Cell Sci.* **124**, 1183-1193.
Woznica, A., Haeussler, M., Starobinska, E., Jemmett, J., Li, Y., Mount, D. and Davidson, B. (2012). Initial deployment of the cardiogenic gene regulatory network in the basal chordate, Ciona intestinalis. *Dev. Biol.* **368**, 127-139.

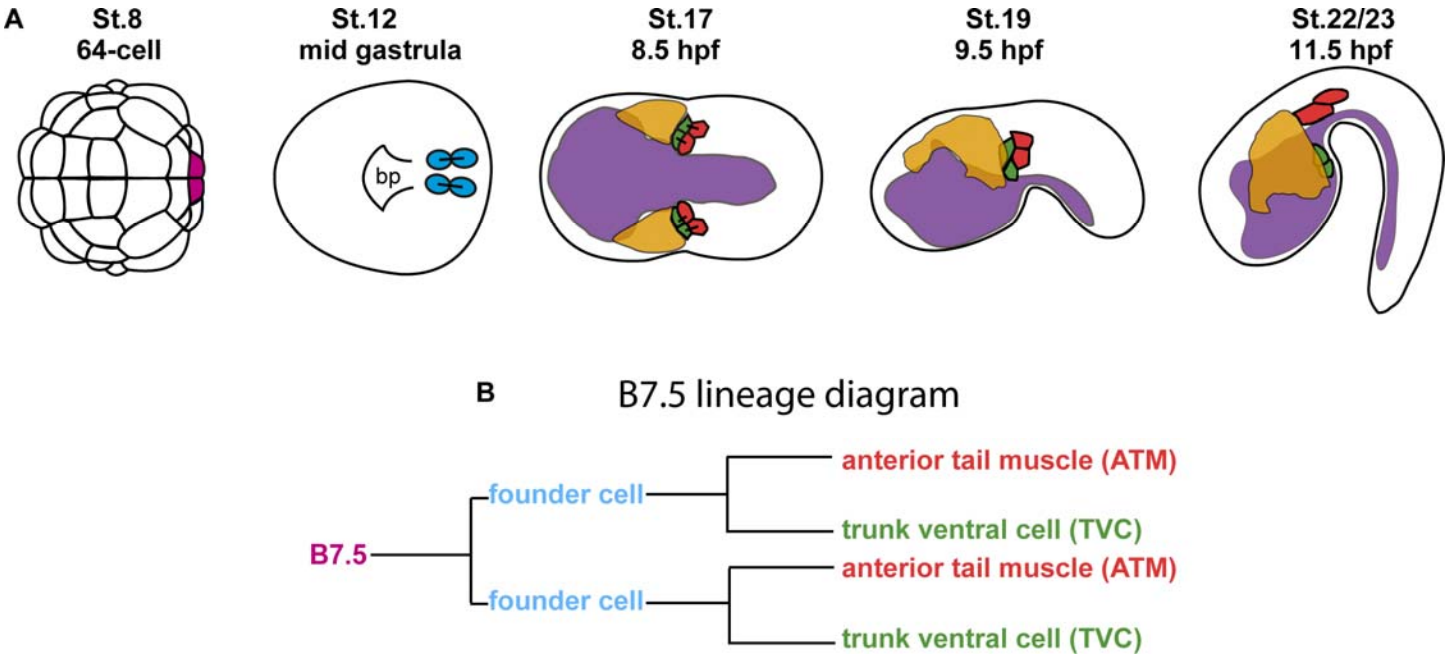

Figure S1. Overview of *Ciona intestinalis* development
(A) Schematic of *Ciona* embryogenesis. Purple; endoderm. Orange; mesenchyme. Magenta; B7.5 cells. Blue; founder cells. Green; TVCs. Red; ATMs. Other tissues were excluded for simplicity. (B) B7.5 lineage diagram.

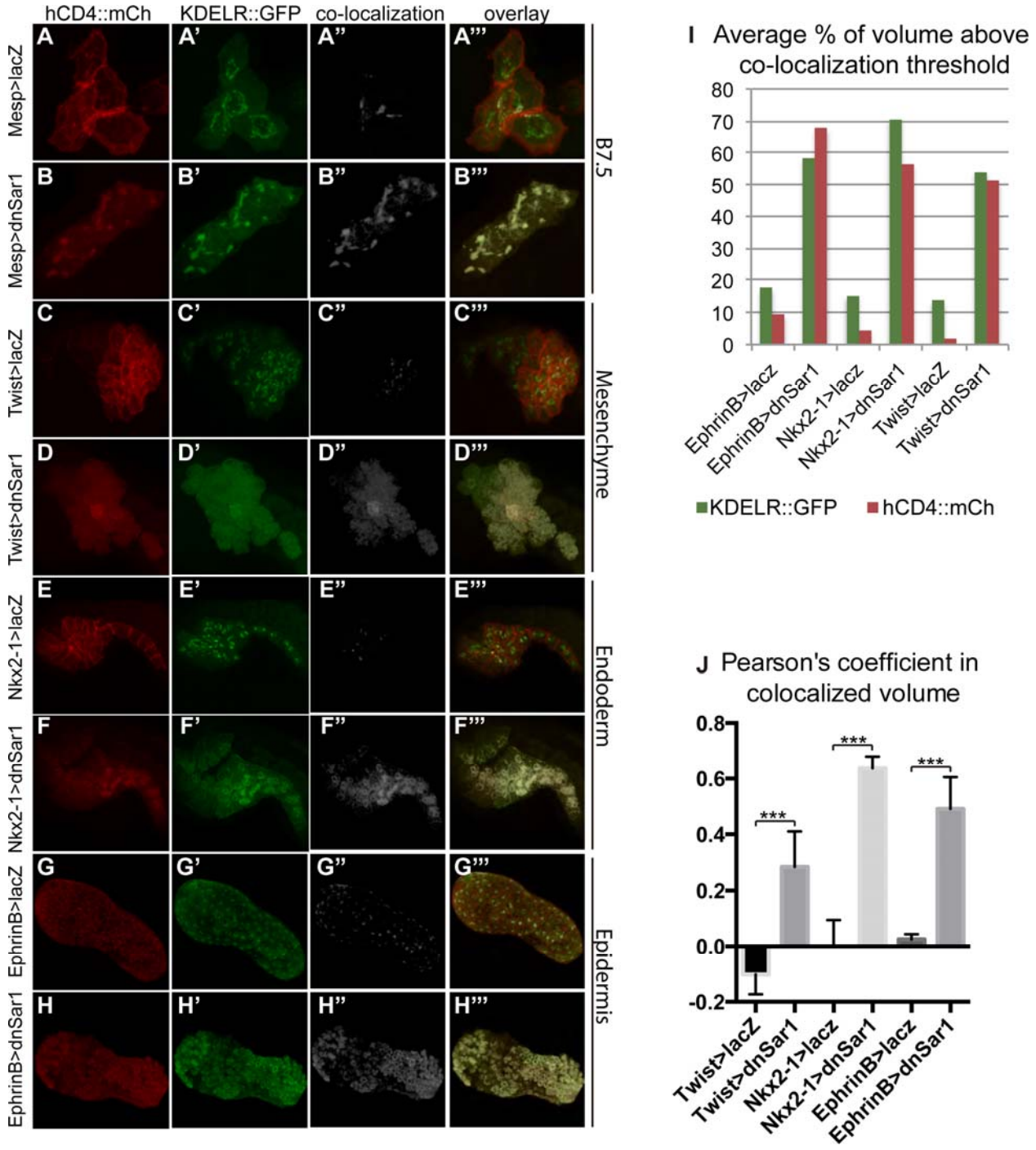

Figure S2. Expression of dnSar1 results in accumulation of hCD4::mCherry in the endoplasmic reticulum.
(A-H”’) Maximal confocal projections of embryos processed in imaris for co-localization (grey) of hCD4::mCherry (red) and KDELR::GFP (green) expressed from indicated drivers on the left, co-expressed with dnSar1 or lacZ as specified. (J) Lines above bars indicate 95% confidence interval. ***P<0.001, one-way ANOVA followed by Tukey’s multiple comparison test.

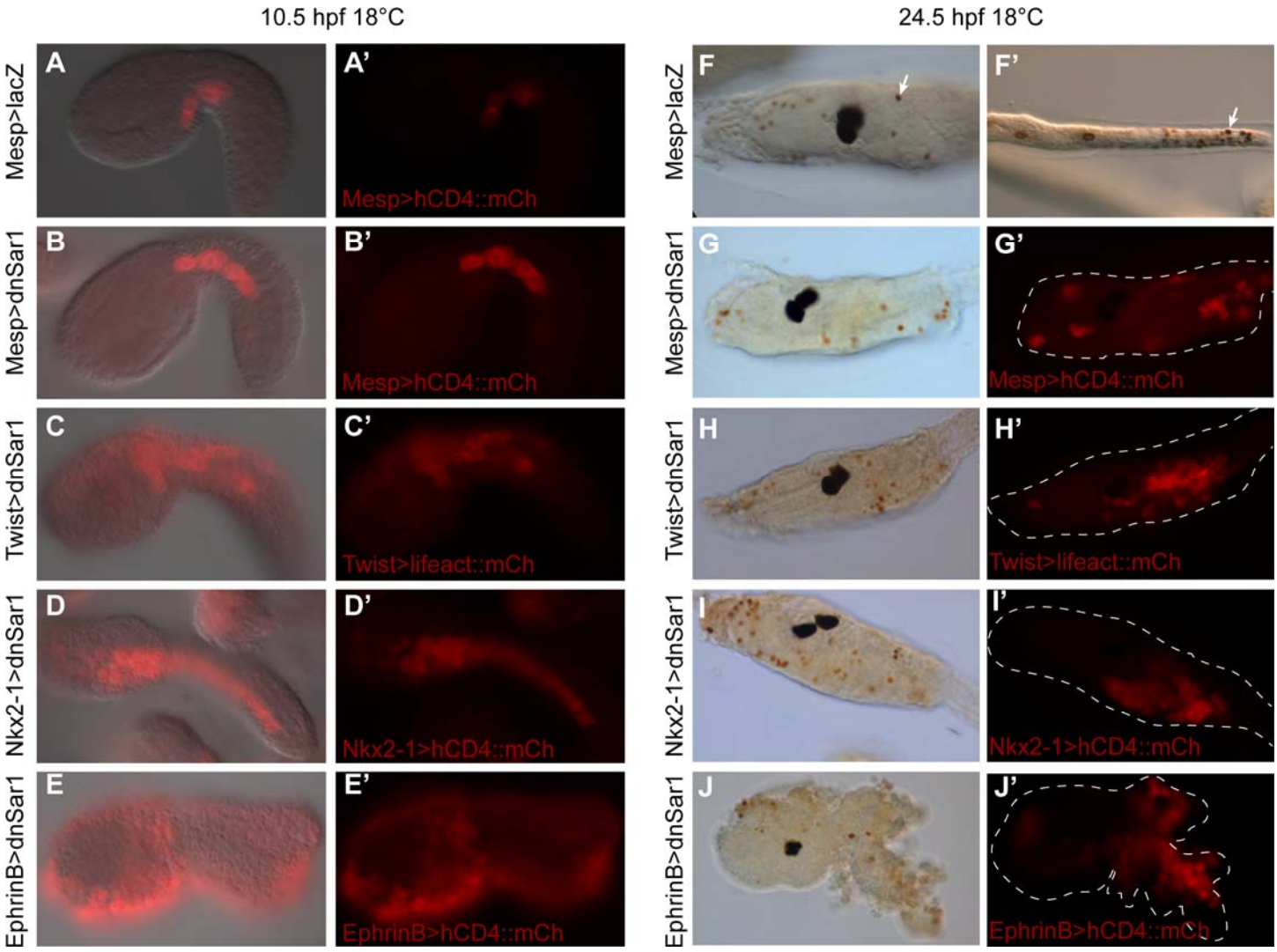

Figure S3. TUNEL staining indicates that dnSar1 expression does not affect cell survival.
(A-J') Embryos expressing lacZ or dnSar1 as indicated on the left, fixed at 10.5 hpf or 24.5 hpf as indicated above. (A, B, C, D and E) Brightfield overlays with epifluorescent images from (A', B', C', D' and E'). (F, F', G, H, I and J) DIC images of embryos electroporated with indicated constructs on left. (G', H', I' and J') Corresponding epifluorescent images of hCD4::mCherry representing dnSar1 expressing cells. fEmbryos outlined in dotted lines. Arrows in F and F' indicate TUNEL positive cells in the trunk and tail epithelium respectively.

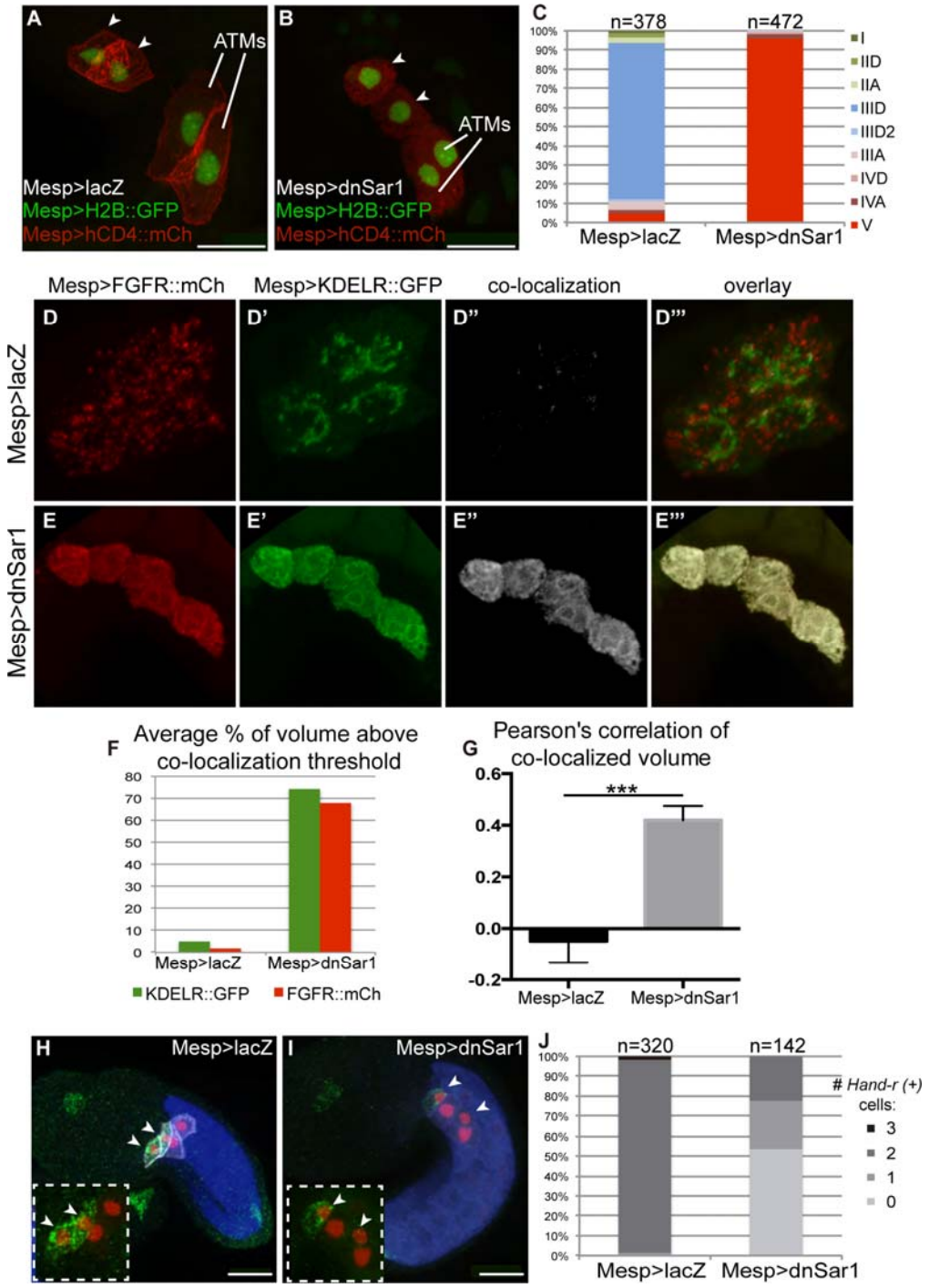

Figure S4. Expression of dnSar1 in the B7.5 lineage disrupts trafficking of FGFR and TVC migration. (A,B) Embryos electroporated with *Mesp>hCD4::mCherry* (red), *Mesp>H2B::GFP* (green) and either *Mesp>dnSar1* or *Mesp>lacZ* as indicated, collected at 12 hpf. (C) Proportions of TVC migration phenotypes in indicated conditions. n, number of electroporated embryo halves scored. (D-E''') Embryos electroporated with *Mesp>FGFR::mCherry* (red), *Mesp>KDELR::GFP* (green) and *Mesp>dnSar1* or *Mesp>lacZ* as indicated and fixed at 10.5 hpf. White indicates co-localization of FGFR::mCherry and KDELR::GFP. (G) Lines above bars indicate 95% confidence interval. ***P<0.001, unpaired t test. (H, I) Embryos stained for *Hand-r* (green) expression, *Mrlc2* (blue) expression, β-galactosidase (red) and hCD4::mCherry (white). White arrows indicate TVCs. (J) Proportions of *Hand-r* expressing cells in indicated conditions. n, number of electroporated embryo halves scored. Arrowheads indicate TVCs. Scale bars represent 25μm.

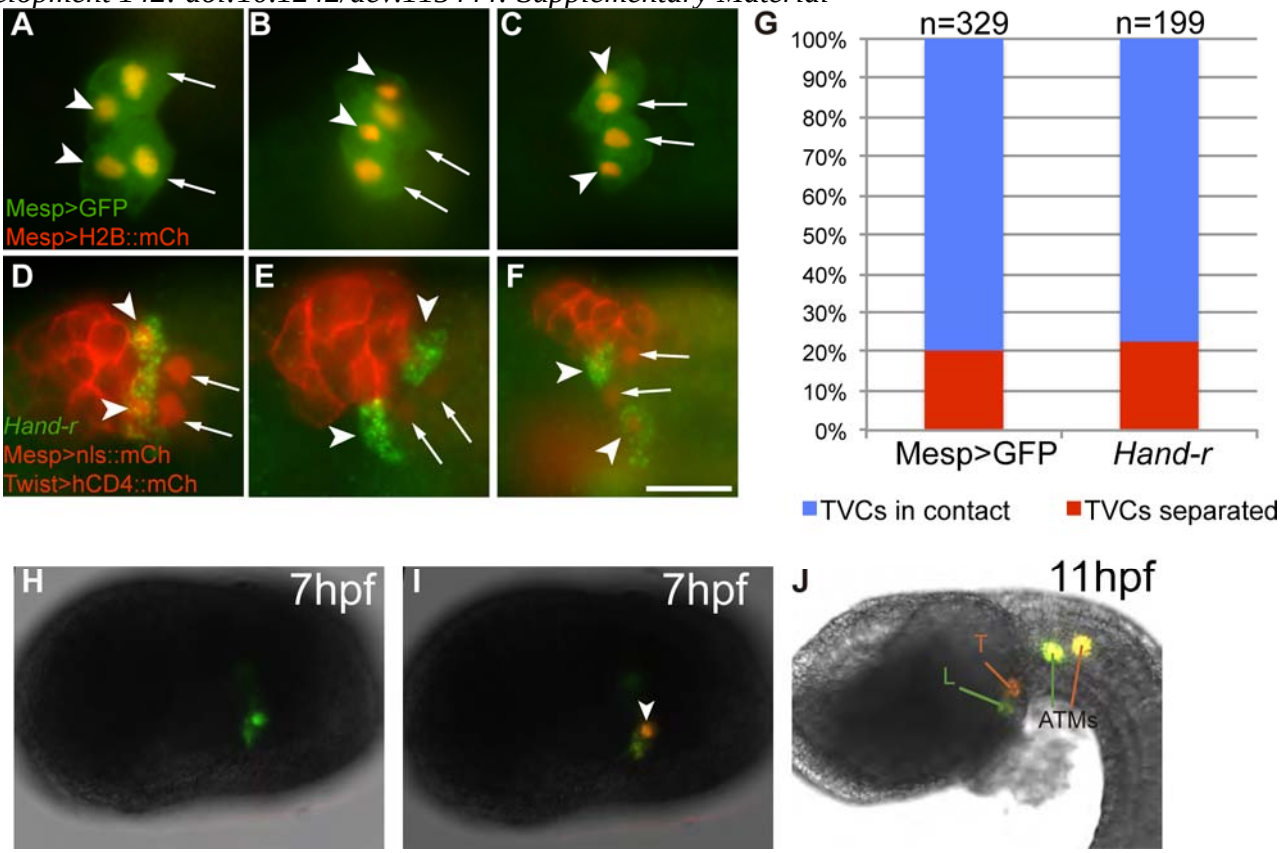

Figure S5. Early TVCs display variable positioning.
(A-C) Epifluorescent images of stage 17 embryos electroporated with *Mesp>GFP* (green) and *Mesp>H2B::mCherry* (red). (D-F) Embryos electroporated with *Twist>hCD4::mCherry* and *Mesp>nls::mCherry*, processed from mCherry immunostaining (red) and in situ hybridization for *Hand-r* (green). (A-F) Arrowheads indicate TVCs. Arrows indicate ATMs. (G) Proportions of TVCs separated or in contact with one another in indicated conditions. n, number of electroporated embryo halves scored. (H-J) Snapshots at indicated timepoints of an embryo electroporated with *Mesp>nls::kaede* (green) which was photoconverted (orange) in the posterior founder cell (arrowhead).

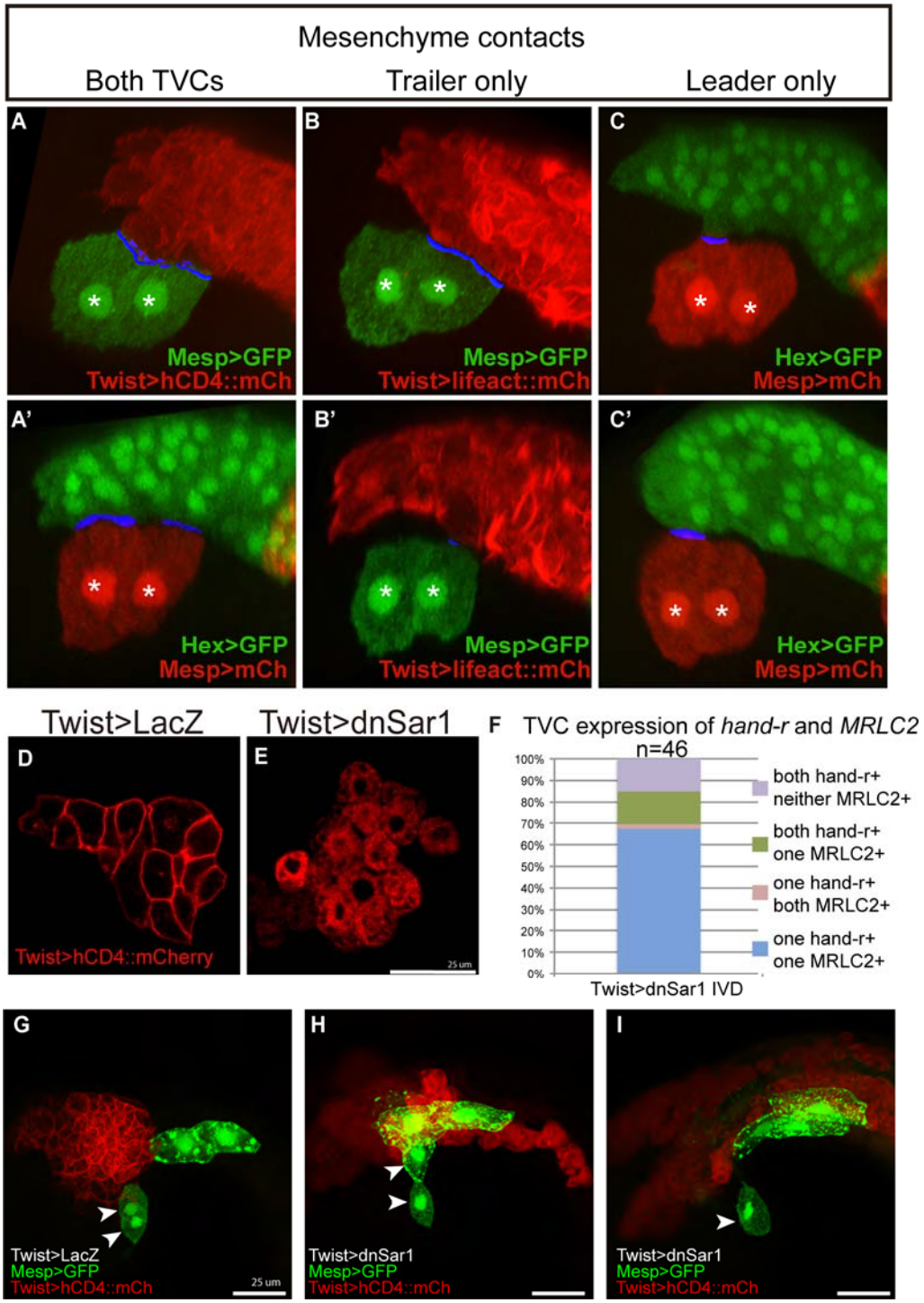

Figure S6. related to Figures 2 and 3. The mesenchyme makes variable and minimal late contact with the TVCs and plays an asymmetrical role in TVC specification.
(A-C') Maximal projections of embryos electroporated with indicated constructs and processed for area of surface contact between the TVCs and mesenchyme (blue). Asterisks indicate TVCs. (D,E) Partial confocal projections of 8.5 hpf embryos electroporated with *Twist>hCD4::mCherry* (red) and *Twist>LacZ* or *Twist>dnSar1* as indicated. (F) Scores for expression of *Hand-r* and Mrlc2 in TVCs of 12 hpf embryos electroporated with Twist>dnSar1 and displaying the IVD phenotype. See Figure 3 (C-D) for more details on the experiment. (G-I) Maximal confocal projections of embryos electroporated with *Twist>hCD4::mCherry* (red), *Mesp>GFP* (green) and *Twist>LacZ* or *Twist>dnSar1* as indicated. White arrowheads indicate TVCs.

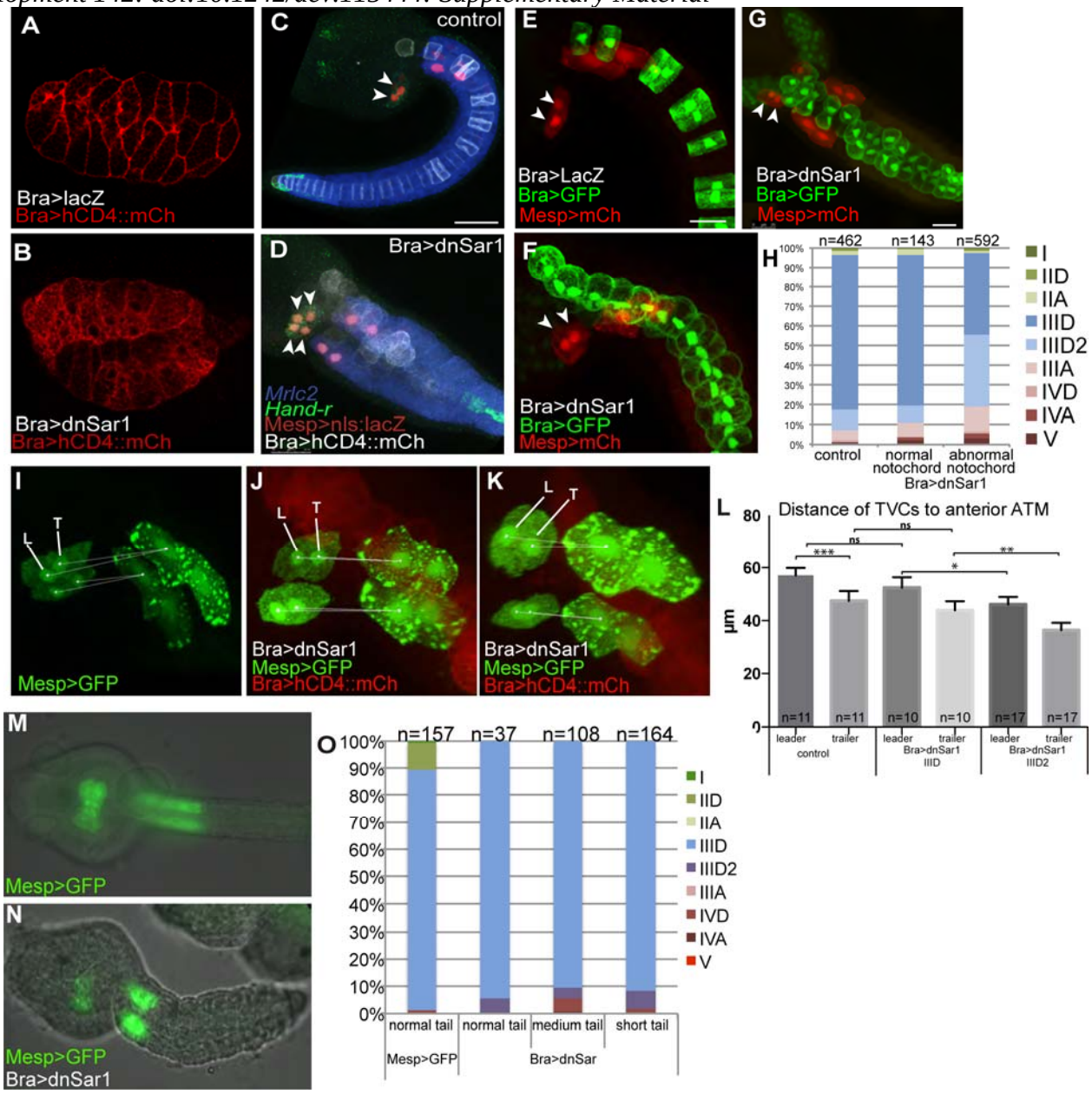

Figure S7. Expression of dnSar1 in the notochord delays the onset of TVC migration.
(A,B) Partial confocal projections of 8.5 hpf embryos electroporated with *Bra>hCD4::mCherry* (red) and *Bra>lacZ* or *Bra>dnSar1* as indicated. (C,D) Maximal confocal projections of 12 hpf embryos electroporated with *Mesp>nls::lacZ* (red), *Bra>hCD4::mCherry* (white) and *Bra>dnSar1* as indicated, processed for double FISH probed for *Hand-r* (green) and *Mrlc2* (blue). (E-G) Maximal confocal projections of embryos electroporated with *Mesp>mCh* (red), *Bra>GFP* and *Bra>dnSar1* as indicated. (H) Proportions of TVC migration phenotypes in indicated conditions. n, number of electroporated embryo halves scored. (I-K) Maximal confocal projections of 12 hpf embryos electroporated with *Mesp>GFP* (green) and (J and K) with *Bra>hCD4::mCherry* (red) and *Bra>dnSar1*. White lines indicate distance from TVC to anterior ATM as measured in Imaris. L; leader, T; trailer. (L) Average distance between indicated TVCs and anterior ATM. Lines above bars indicate 95% confidence interval. n.s., not significant; *P<0.05, **P<0.01, ***P<0.001, one-way ANOVA followed by Tukey's multiple comparison test. (M,N) Epifluorescent images of embryos electroporated with *Mesp>GFP* raised until 15hpf. (O) Proportions of TVC migration phenotypes in indicated conditions scored at 15 hpf. n, number of electroporated embryo halves scored. Arrowheads indicate TVCs.

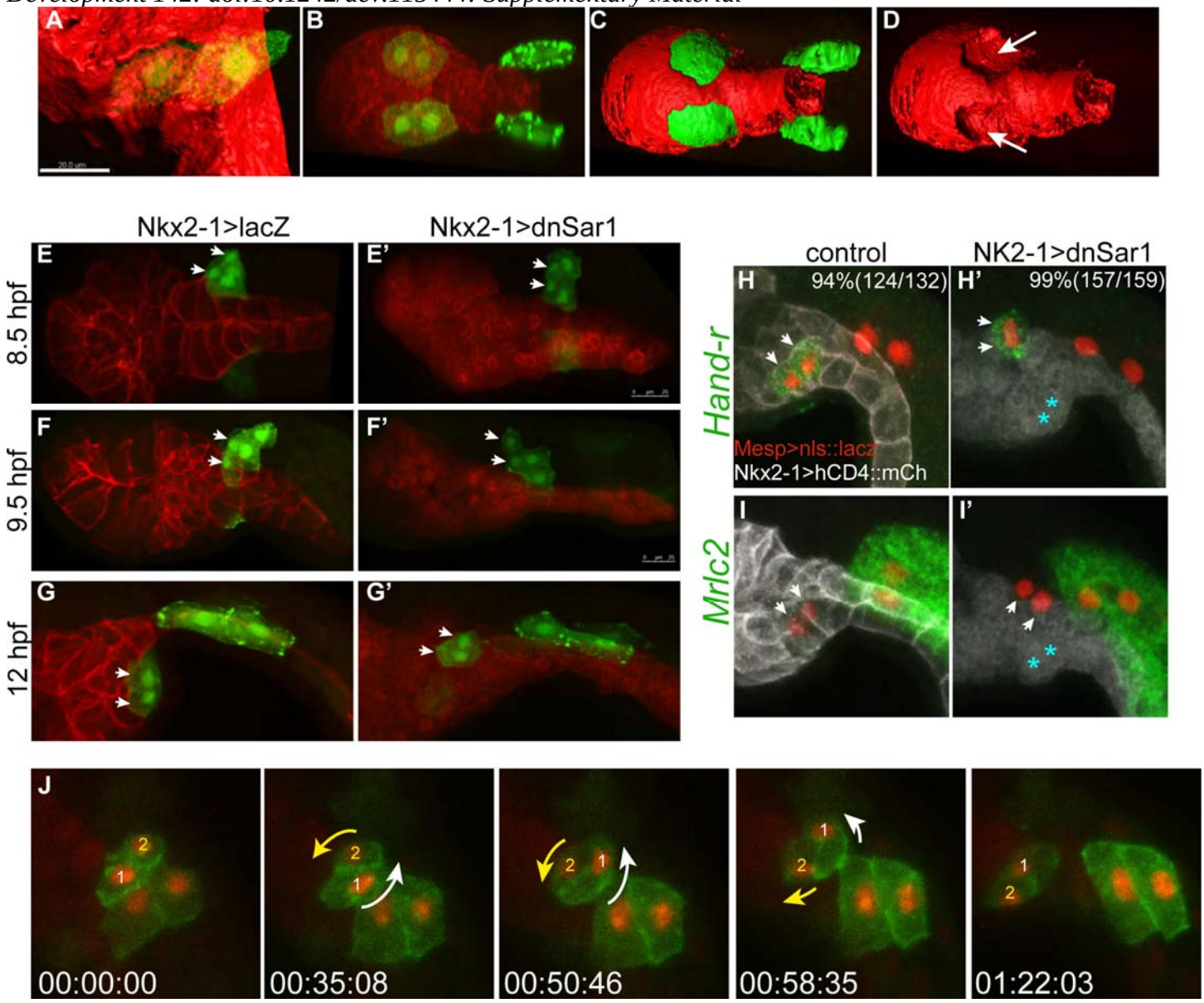

Figure S8. related to Figure 4. The endoderm is required for leader-trailer polarity and ventral migration.

(A-G') Maximal confocal projections of embryos electroporated with *Nkx2-1>hCD4::mCherry* (red), *Mesp>GFP* (green) and *Nkx2-1>lacZ* or *Nkx2-1>dnSar1* as indicated. (A) 10 hpf embryo with surface of hCD4:mCherry rendered in Imaris. (B-D) Ventral view of an embryo raised to 12 hpf, with hCD4::mCherry (red) and GFP (green) rendered in imaris. Endodermal pockets where the TVCs sit indicated by arrows. (H-I') Maximal confocal projections of 12 hpf embryos electroporated with *Nkx2-1>hCD4::mCherry* (white), *Mesp>nls::lacZ* (red) and *Nkx2-1>dnSar1* as indicated and processed for *Hand-r* or *Mrlc2* FISH (green). (H,H') Percentage of embryo halves scored with both TVCs expressing *Hand-r* indicated on top right. (J) Maximal projections of stills from a time-lapse of an embryo electroporated with *Mesp>GFP* (green), *Mesp>H2B::mCherry* (red), *Nkx2-1>hCD4::mCherry* (red) and *Nkx2-1>dnSar1*. TVCs labeled 1 and 2. Arrows represent direction of migration of each TVC; arrow color corresponds to number color. Arrowheads indicate TVCs. Timestamp, hours:minutes:seconds.

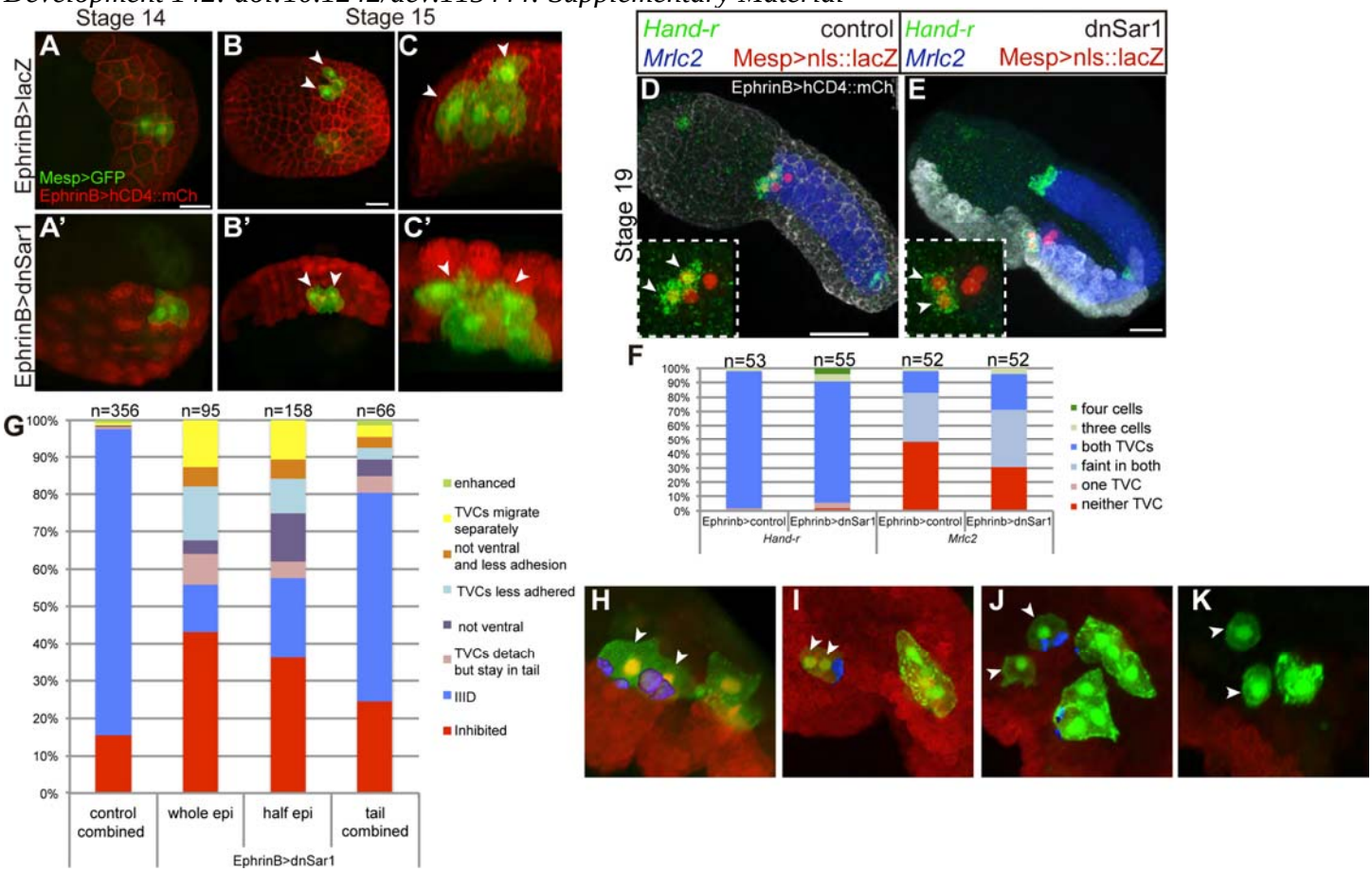

Figure S9. related to Figure 5. Signaling from the epidermis is required for TVC-TVC and TVC-ECM adhesions.

(A-C', H-K) Maximal confocal projections of embryos fixed at indicated stages, electroporated with *Mesp>GFP* (green), *EphrinB>hCD4::mCherry* (red), and *EphrinB>lacZ* or *EphrinB>dnSar1*. (A-B') ventral views. (C-C') transverse section at the level of the TVCs. (D, E) Maximal confocal projections of stage 19 embryos electroporated with *Mesp>nls::lacZ* (red), *EphrinB>hCD4::mCherry* (white) and *EphrinB>dnSar1* as indicated, and processed for double FISH probed for *Hand-r* (green) and *Mrlc2* (blue) expression. Boxed regions show magnified views of the B7.5 lineage and *Hand-r* expression. (F) Proportions of the number of cells expressing *Hand-r* or *MRLC2* per embryo half in indicated conditions. n, number of embryo halves scored. (G) Proportions of TVC migration phenotypes including non-standard categories. n, number of electroporated embryo halves. (H-K) 12 hpf embryos electroporated with *EphrinB>dnSar1* and processed in Imaris for area of surface contact between the TVCs and epidermis (blue). White arrowheads indicate TVCs.

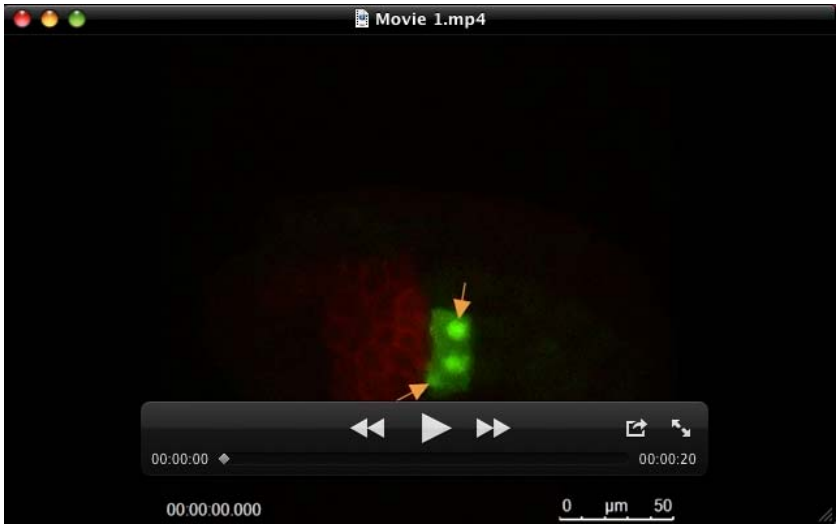

Movie 1. Normal TVC migration
Timelapse of an embryo electroporated with Mesp>GFP (green) and Twist>hCD4::mCherry (red). In this and all subsequent movies, orange arrows indicate TVCs, blue arrows indicate ATMs, L indicates leader, T indicates trailer and the timestamp is in hours:minutes:seconds:miliseconds. Lateral view with anterior to the left.

Movie 2. The trailer TVC migrates independently of the stalled leader TVC expressing dnSar1
Timelapse of an embryo electroporated with Mesp>GFP (green), FoxF(TVC)>H2B::mCherry (red) and FoxF(TVC)>dnSar1. The TVC in the trailer position (orange arrow) migrates around the TVC in the leader position (red arrow) which is stalled due to expression of dnSar1 as assayed by H2B::mCherry expression. Lateral view with anterior to the right.

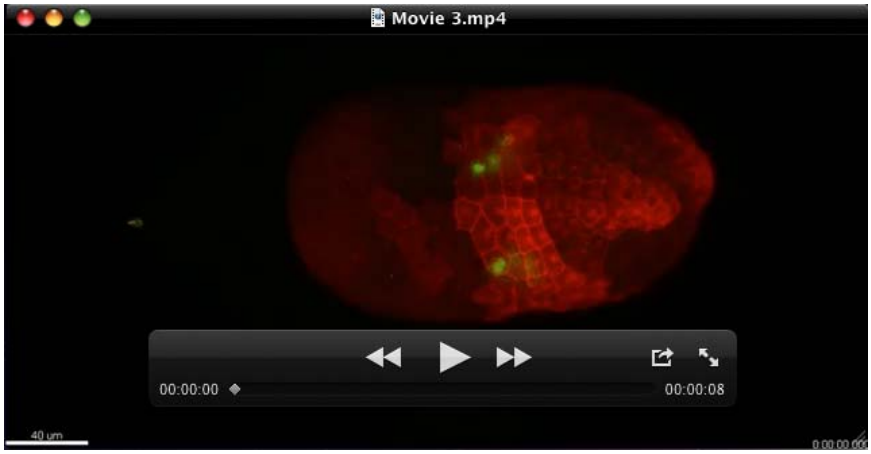

Movie 3. Initially separated TVCs come into contact during migration
Timelapse of an embryo electroporated with EphrinB>hCD4::mCherry (red) and Mesp>H2B::GFP (green). Anterior is to the left.

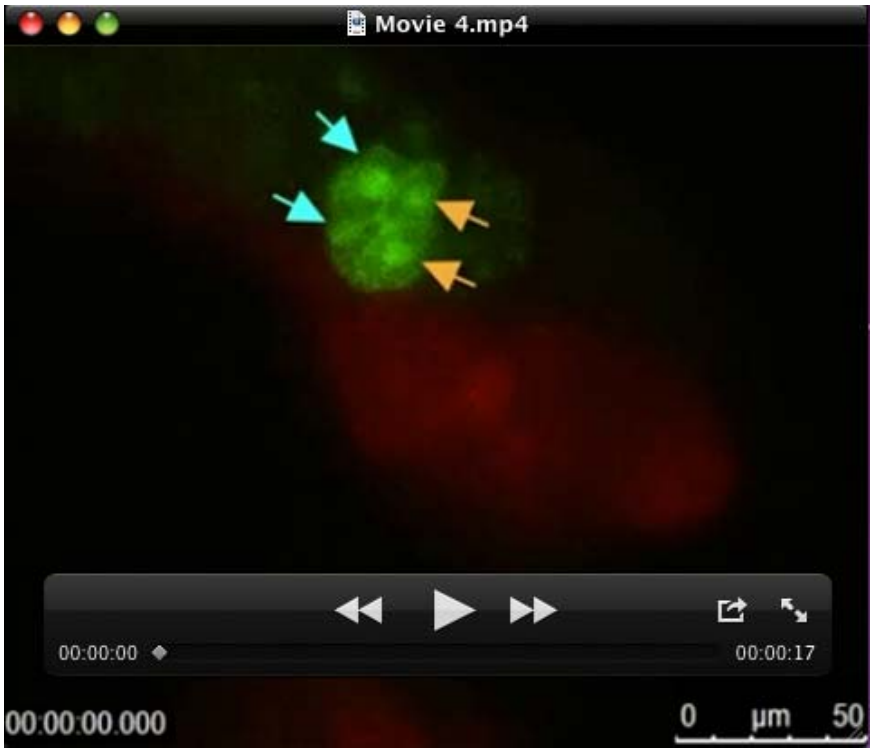

Movie 4. TVCs switch positions in the absence of signaling from the endoderm
Timelapse of an embryo electroporated with Mesp>GFP (green), Nkx2-1>hCD4::mCherry (red) and Nkx2-1>dnSar1. Lateral view with anterior to the right.

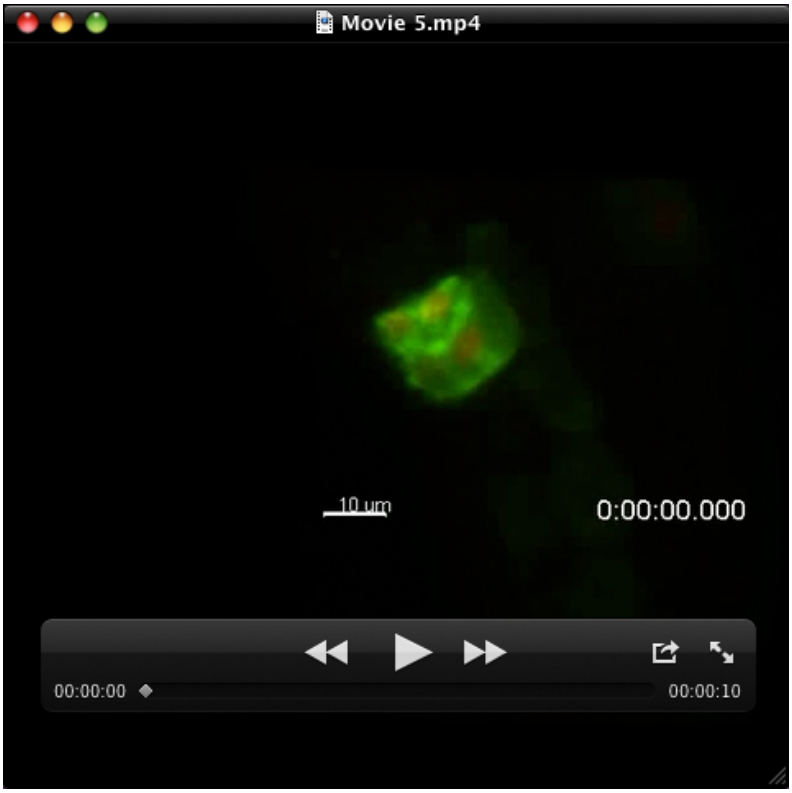

Movie 5. TVCs switch positions in the absence of signaling from the endoderm
Timelapse of an embryo electroporated with Mesp>lifeact::GFP (green), Mesp>H2B::mCherry (red) and Nkx2-1>dnSar1. Lateral view with anterior to the left.

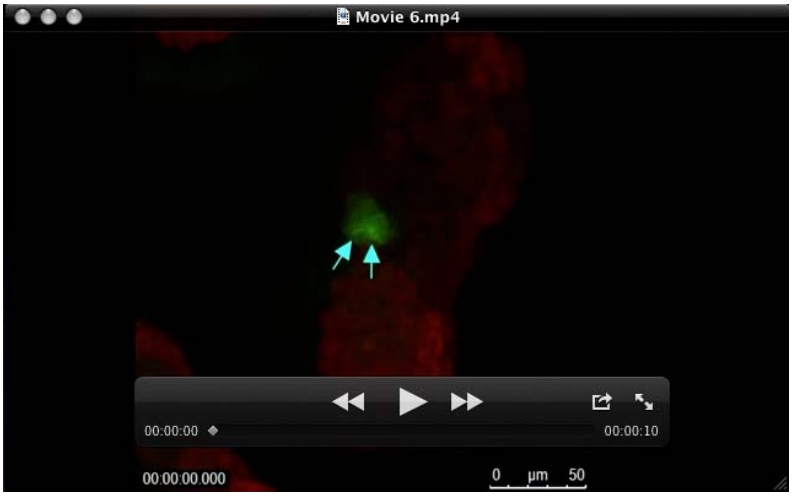

Movie 6. TVCs migrate along the dorsal midline in the absence of signaling from the epidermis
Timelapse of an embryo electroporated with Mesp>GFP (green), EphrinB>hCD4::mCherry (red) and EphrinB>dnSar1. Lateral view with anterior to the top.

Movie 7. TVCs exhibit staggered migration in the absence of signaling from the epidermis
Timelapse of an embryo electroporated with Mesp>GFP (green), EphrinB>hCD4::mCherry (red) and EphrinB>dnSar1. Anterior is to the bottom right.

Table S1. Primers used to amplify enhancers used in this study from *Ciona intestinalis* genomic DNA. Numbers indicate distance in base pairs from the start codon.

Nkx2-1 -2680Asc1F	AAAGGCGCGCCCATGGCGTCGTGTGTACTTCT
Nkx2-1 -1Not1R	TTTGCGGCCGCCTCACAGCAAAGTTTCCAGTG
EphrinB -2934 Asc1F	ACAGGCGCGCCCGTCGTGCTAACGGTATACCA
EphrinB -1Not1R	TGTGCGGCCGCTCTCTCCAGGTGCTGTGGTGT
Hex -2787Xba1F	TGTTCTAGATGTGTACAGCCACCTTGAATCGT
Hex -7Not1R	AAAGCGGCCGCAGAAGTTCTAGGATAGGTGTTTGG

We used a modified form of the Brachyury enhancer from (Corbo et al., 1997) which included a stop codon in each reading frame after the short stretch of Brachyury coding sequence.